HIGHER-ORDER HYBRID-PATTERN SOLITONS ON THE n-PERIODIC BACKGROUND FOR THE REVERSE-SPACE-TIME DERIVATIVE NONLINEAR SCHRÖDINGER EQUATION

HUIJUAN ZHOU, YONG CHEN*, XIAOYAN TANG, AND YUQI LI

Abstract. The Darboux transformation formulae for the reverse-space-time derivative nonlinear Schrödinger equation are given by using concise expressions. At the same time, the n-solitons, n-periodic solutions, higher-order hybrid-pattern solitons and some mixed solutions are obtained through Darboux transformation formulae. It's worth mentioning that the solution of reverse-space-time DNLS equation can be reduced to the solution of local DNLS equation by symmetry relation. In the case of zero seed solution, the fact that solution $q[N]$ at origin depends only on the spectral parameters is proved. Also, the amplitudes of n-solitons, n-periodic solutions, higher-order solitons and mixed solutions are derived. Moreover, many interesting new phenomena are discovered through detailed dynamic analysis of these solutions. For example, interactions of n-periodic waves produce peaks with different amplitudes and size. Soliton on the periodic background looks very similar to breathers due to the interception of the periodic background. Finally, the modulational instability analysis for the reverse-space-time derivative nonlinear Schrödinger equation is studied. The results are useful for describing the interaction process of solitons interference by n-periodic waves in the ocean and other fields.

Keywords:Darboux transformation; Reverse-space-time derivative nonlinear Schrödinger equation; n-periodic solution; High-order hybrid-pattern solitons on the n-periodic background.

1. Introduction

Starting from the Kaup-Newell system [1–5]:

$$\begin{aligned} iq_t - q_{xx} - i(q^2 r)_x = 0, \\ ir_t + r_{xx} - i(qr^2)_x = 0. \end{aligned} \tag{1.1}$$

When $r(x,t) = -q^*(x,t)$, the derivative nonlinear Schrödinger equation (DNLS) [6–9]

$$iq_t - q_{xx} + i(q^2 q^*)_x = 0, \tag{1.2}$$

is derived from the Kaup-Newell system and the integrability of DNLS was proved by Kaup and Newell in 1978. The DNLS equations arise in the study of circular polarized Alfvén waves in plasma [10], propagating parallel to the magnetic field [11], which is one of the most important integrable systems in mathematics and physics. Here in Eq.(1.2) the complex function $q = q(x,t)$ denotes the wave envelopes, the superscript $*$ denotes complex conjugation and the subscripts x and t denote the partial derivatives with respect to x and t, respectively. In nonlinear optics, the DNLS is gauge equivalent to the modified nonlinear Schrödinger equation, which has important physical significance in the theory of ultrashort femtosecond nonlinear pulse [12]. In addition, the filamentation of lower-hybrid waves can be simulated by the DNLS which governs the asymptotic state of the filamentation, and it admits moving solitary envelope solutions for the electric field [13]. Ichikawa et al. [14] obtained the peculiar structure of spiky modulation of amplitude and phase, which arises from the derivative nonlinear coupling term. The equation is also used to describe large-amplitude magnetohydrodynamic waves of plasmas [15, 16], the sub-picosecond and femtosecond pulses in single-mode optical fiber [17–19].

Due to generating many new physical phenomena and having important physical significance when nonlocal terms are added to nonlinear equations, the nonlocal equations have been studied by many researchers from different viewpoints and perspectives in recent years [20–22]. The PT-symmetric, reverse-time and reverse-space-time nonlocal DNLS are three types nonlocal DNLS equations which were first proposed by Ablowitz and Musslimani [23, 24]. Among them, the reverse-space-time DNLS equation is as follows

$$iq_t - q_{xx} + i(q^2 q(-x,-t))_x = 0, \tag{1.3}$$

which is derived from the Kaup-Newell system with $q(x,t) = -r(-x,-t)$. The symmetry reductions of reverse-space-time DNLS equation are nonlocal both in space and time. Note that the Lax pair of Kaup-Newell systems is

$$\Psi_x = U\Psi, \quad \Psi_t = V\Psi.$$

The eigenfunction $\Psi = \begin{pmatrix} \phi_k \\ \varphi_k \end{pmatrix}$ associated with eigenvalue λ_k. U and V are functional matrices with spectral parameters λ_k. Under the different reduction conditions, the symmetry relation of eigenfunctions are also different. The reverse-space-time DNLS equation has the following property [7]:

$$\phi_k(x,t;\lambda_k) = \varphi_k(-x,-t;\lambda_k).$$

For the DNLS equation, the eigenfunctions admit the following symmetry conditions:
(i): $\lambda_k = -\lambda_k^*$, $\phi_k^* = \varphi_k$;
(ii): $\lambda_k^* = -\lambda_l$, $\phi_k^* = \varphi_l$, $\varphi_k^* = \phi_l$, where $k \neq l$.

From the symmetry relation between DNLS equation and reverse-space-time DNLS equation, it can be seen that the solution of DNLS equation is also the solution of reverse-space-time DNLS equation. Therefore, in this paper, we study reverse-space-time DNLS equation instead of DNLS or other types of nonlocal DNLS equation. The reverse-space-time DNLS equation has many physical applications in optics, ocean water waves, quantum entanglement and an unconventional system of magnetics and so on [25]. The solution of reverse-space-time DNLS equation can extend the solution of the local equation to a more general case and deepen the physical research.

In 1965, Kruskal and Zabusky studied the entire process of the interaction between two soliton waves of the KdV equation in detail and found that the solitary waves had the properties of elastic collision [30]. Except for the elastic collision, resonance of solitons is also an important natural phenomenon which may lead to a disaster. Some important results of soliton solutions of DNLS equation have been derived by different approaches. With the help of the Hirota bilinear transformation method [31], the N-soliton formula of the DNLS was constructed by Nakamura and Chen. Huang and Chen established the determinant form of N-soliton formula based on Darboux transform (DT) technique [32]. Kamchatnov etc. studied the formation of solitons on the sharp front of optical pulse in an optical fiber according to the DNLS equation [34]. The compact N-soliton formulae with both asymptotically vanishing and nonvanishing amplitudes were obtained by iterating Bäcklund transformation of the DNLS equation [35]. High-order solitons of DNLS equation were studied by the generalized DT [36]. Multi-solitons of three-component coupled DNLS equation were constructed in [37].

In 1987, exact representations of double-periodic solutions were constructed in [39] by separating the variables and reducing the NLS equation to the first-order quadratures. In 2012, Hu, Lou and Chen derived cnoidal periodic wave solution by nonlocal symmetries [40]. He and Tao et.al obtained periodic background of variable coefficients integrable equation in [41]. In 2014, Kedziora, Ankiewicz and Akhmedie constructed rogue waves and solitons on a cnoidal background [42]. Huang and Ling constructed periodical solutions by PT symmetry in 2016 [43]. In 2017, Zhao and Ling et al. studied rogue wave excitation pattern in a two-component Bose-Einstein condensate with pair-transition effects. The results indicate that rogue wave excitation can exist on a stripe phase background for which there are cosine and sine wave background in the two components respectively [44]. In [45], Chen and Pelinovsky constructed two families of travelling periodic waves of the mKdV equation in the focusing case expressed by the Jacobian elliptic functions dn and cn. In [46], Liu, Zhang and He constructed the rogue waves on the periodic background by using generalized odd-order DT. Xue etc. studied breathers and breather-rogue waves on a periodic background for the DNLS equation [47]. In [48], Zhou and Chen constructed the double-periodic by DT with a plane wave seed solution.

In the ocean, the surface of the ocean is usually in the form of quasi-periodic waves due to the motion of the ocean and other factors. Obviously, pure soliton interactions only appear in the lab, in the complicated natural environment, interaction process of solitons are often interference by other waves, such as: the periodic waves. European Space Agency image of waves in Hudson Bay on July 18,1992. In addition to the most obvious grid soliton wave with periodic waves, there are two newly generated bar solitary waves, a boat and its tail wave. SAR image of the Mediterranean Sea near the Strait of Gibraltar taken by the European Space Agency on July 19, 1994. It shows a family of solitons with a quasi-periodic background curve on the Mediterranean side of the Strait of Gibraltar, propagating in the direction of the Alboran Sea. The large packet of solitons with quasi-periodic waves radiating eastward from the Strait of Gibraltar, having been formed by intense westward tidal flow across the Camarinal Sill several hours earlier. The ocean solitary waves in [38] are obviously not simple elastic collisions, but solitary wave motions under quasi-periodic wave background interference, so studying the solitons on the n-periodic background can better reflect the real situation.

In this investigation, the DT formulae are given by using concise expressions. Then giving a zero seed solution, the solution $q[N]$ obtained by N-fold DT at origin is equal to $-2i\sum_{j=1}^{N}\lambda_j$, which depends only on the spectral parameters is proved. Solitons(including elastic collision and velocity resonance solitons), periodic solution and multi-soliton on the n-periodic background are constructed by the even-fold DT. Higher-order soliton and higher-order soliton on the n-periodic background are constructed by degenerate DT and semi-degenerate DT. The higher-order hybrid-pattern solitons and higher-order hybrid-pattern solitons on the n-periodic background are constructed by generalized degenerate and semi-degenerate DT. Also the amplitudes of m-solitons, n-periodic solutions, higher-order solitons and mixed solutions are derived. Moreover, many interesting new phenomena are discovered through dynamic analysis of these solutions and the analysis for these phenomena are given in detail. In particular, the periodic solutions and soliton solutions can be transformed into zero solution when $\sum_{j=1}^{N}\lambda_j = 0$. We also give the Modulation instability (MI) for the Reverse-space-time DNLS equation. These results would also be useful for understanding the corresponding soliton phenomena in many fields of local and nonlocal nonlinear dynamical systems such as ocean, nonlinear optics, Bose-Einstein condensates and other relevant fields [49–54].

The organizational structure of this paper is as follows. In Section 2, multi-solitons on the n-periodic background are given by N-fold DT formula. Higher-order solitons on the n-periodic backgrounds are obtained by the semi-degenerate DT formula in Section 3. In Section 4, we construct high-order hybrid-pattern solitons on the n-periodic background by generalized semi-degenerate DT formula. In Section 5, modulation instability analysis of reverse-space-time DNLS equation is given. The final section is devoted to conclusion.

2. Multi-solitons on the n-periodic background

The Lax pair of reverse-space-time DNLS equation is shown as follows.

$$\Psi_x = \left(i\sigma\lambda^2 + Q\lambda\right)\Psi = U\Psi, \tag{2.1}$$

$$\Psi_t = \left(2i\sigma\lambda^4 + V_3\lambda^3 + V_2\lambda^2 + V_1\lambda\right)\Psi = V\Psi, \tag{2.2}$$

with

$$\Psi = \begin{pmatrix} \phi \\ \varphi \end{pmatrix}, \quad \sigma = \begin{pmatrix} 1 & 0 \\ 0 & -1 \end{pmatrix}, \quad Q = \begin{pmatrix} 0 & q \\ -q(-x,-t) & 0 \end{pmatrix},$$
$$V_3 = 2Q, \quad V_2 = iQ^2, \quad V_1 = Q^3 + iQ_x\sigma.$$

The spectral parameter λ is an arbitrary complex number, Ψ is the eigenfunction corresponds to λ. The symmetric relation of the eigenfunction corresponding to the spectrum problem Eq.(2.1) and Eq.(2.2) given in the form of lemma.

Lemma 1. *Introducing* $\Psi_j = \begin{pmatrix} \phi_j \\ \varphi_j \end{pmatrix} = \begin{pmatrix} \phi_j(x,t,\lambda_j) \\ \varphi_j(x,t,\lambda_j) \end{pmatrix}, j = 1, 2, \ldots,$ *which is the eigenfunction of the Lax pair* (2.1) *and* (2.2) *associated with* $\lambda = \lambda_j$. *The eigenfunction admit the following symmetry condition:*

$$\begin{pmatrix} \phi(x,t;\lambda_j) \\ \varphi(x,t;\lambda_j) \end{pmatrix} = \begin{pmatrix} \varphi(-x,-t;\lambda_j) \\ \phi(-x,-t;\lambda_j) \end{pmatrix}. \tag{2.3}$$

The eigenfunctions admit the following symmetry condition:

$$\begin{pmatrix} \phi(x,t;\lambda_j) \\ \varphi(x,t;\lambda_j) \end{pmatrix} = \begin{pmatrix} \varphi(-x,-t;\lambda_j) \\ \phi(-x,-t;\lambda_j) \end{pmatrix},$$

where $\begin{pmatrix} \phi(x,t;\lambda_j) \\ \varphi(x,t;\lambda_j) \end{pmatrix}$ is an eigenfunction associated with $\lambda = \lambda_j$.

Proof. Form the x part of the Lax pair Eq.(2.1) and Eq.(2.2), one has

$$\begin{pmatrix} \phi(x,t;\lambda_j) \\ \varphi(x,t;\lambda_j) \end{pmatrix}_x = \begin{pmatrix} i\lambda_j^2 & q(x,t)\lambda_j \\ -q(-x,-t)\lambda_j & -i\lambda_j^2 \end{pmatrix}\begin{pmatrix} \phi(x,t;\lambda_j) \\ \varphi(x,t;\lambda_j) \end{pmatrix}.$$

Let $x = -x$, $t = -t$ then

$$\begin{pmatrix} \phi(-x,-t;\lambda_j) \\ \varphi(-x,-t;\lambda_j) \end{pmatrix}_x = \begin{pmatrix} -i\lambda_j^2 & -q(-x,-t)\lambda_j \\ q(x,t)\lambda_j & i\lambda_j^2 \end{pmatrix}\begin{pmatrix} \phi(-x,-t;\lambda_j) \\ \varphi(-x,-t;\lambda_j) \end{pmatrix},$$

or

$$\begin{pmatrix} \varphi(-x,-t;\lambda_j) \\ \phi(-x,-t;\lambda_j) \end{pmatrix}_x = \begin{pmatrix} i\lambda_j^2 & q(x,t)\lambda_j \\ -q(-x,-t)\lambda_j & -i\lambda_j^2 \end{pmatrix}\begin{pmatrix} \varphi(-x,-t;\lambda_j) \\ \phi(-x,-t;\lambda_j) \end{pmatrix}.$$

So

$$\begin{pmatrix} \varphi(-x,-t;\lambda_j) \\ \phi(-x,-t;\lambda_j) \end{pmatrix} \textit{and} \begin{pmatrix} \phi(-x,-t;\lambda_j) \\ \varphi(-x,-t;\lambda_j) \end{pmatrix}$$

satisfy the same spectral problem. Taking a similar procedure, the symmetry proper also holds for the t part of the Lax pair. That means, if $\begin{pmatrix} \phi(x,t;\lambda_j) \\ \varphi(x,t;\lambda_j) \end{pmatrix}$ is the eigenfunction of Eq.(2.1) and Eq.(2.2) corresponding to λ_j, then so is $\begin{pmatrix} \varphi(-x,-t;\lambda_j) \\ \phi(-x,-t;\lambda_j) \end{pmatrix}$. □

Considering the gauge transformation

$$\Psi[N] = T\Psi, \tag{2.4}$$

the spectral problem (2.1) and (2.2) are transformed to

$$\begin{aligned} \Psi[N]_x &= U[N]\Psi[N], \quad U[N] = U|_{q(x,t)\to q[N](x,t),q(-x,-t)\to q[N](-x,-t)}, \\ \Psi[N]_t &= V[N]\Psi[N], \quad V[N] = V|_{q(x,t)\to q[N](x,t),q(-x,-t)\to q[N](-x,-t)}. \end{aligned} \tag{2.5}$$

Based on the Eq. (2.5), the following conclusions are given

$$T_x = U[N]T - TU, \tag{2.6}$$

$$T_t = V[N]T - TV. \tag{2.7}$$

Furthermore, the following identity is deduced

$$U[N]_t - V[N]_x + [U[N], V[N]] = T(U_t - V_x + [U,V])T^{-1}. \tag{2.8}$$

That is, the same equation (1.3) is derived with $q(x,t) \to q[N](x,t)$, where $q[N]$ in the spectral problem (2.5) is also a solution of Eq. (1.3).

DT can construct solutions of the integrable equation by pure algebraic construction, which has unique advantage in solving integrable equations. To construct the N-fold DT of Eq.(1.3), we consider the Darboux matrix T in Eq. (2.4) in the form

$$T = \sum_{\ell=0}^{[\frac{N}{2}]} \begin{pmatrix} a_{N-2\ell}\lambda^{N-2\ell} & b_{N-2\ell-1}\lambda^{N-2\ell-1} \\ c_{N-2\ell-1}\lambda^{N-2\ell-1} & d_{N-2\ell}\lambda^{N-2\ell} \end{pmatrix}.$$

Where $[\frac{N}{2}]$ is a least integer function, a_0, b_0, c_0 and d_0 are constants. When the subscripts of $a_{N-2\ell}$, $b_{N-2\ell-1}$, $c_{N-2\ell-1}$ and $d_{N-2\ell}$ less than zero, the elements are zero, other elements of matrix T are functions about x and t.

Considering the kernel problem of DT matrix T i.e.,

$$T|_{\lambda=\lambda_j} \Psi_j = \sum_{\ell=0}^{[\frac{N}{2}]} \begin{pmatrix} a_{N-2\ell}\lambda_j^{N-2\ell} & b_{N-2\ell-1}\lambda_j^{N-2\ell-1} \\ c_{N-2\ell-1}\lambda_j^{N-2\ell-1} & d_{N-2\ell}\lambda_j^{N-2\ell} \end{pmatrix} \Psi_j = 0, j = 1, 2, \cdots, N. \tag{2.9}$$

Using Cramer's rule, the concrete expression of the new solution $q[N]$ can be seen in the theorem as below.

Theorem 2. *The solution $q[N]$ for the Eq. (1.3) is given in the following N-fold DT formula.*

$$q[N] = \frac{|M^2|}{|P^2|} q + 2i \frac{|MH|}{|P^2|}, \tag{2.10}$$

where $M = (M_{jk})_{1\le j,k\le N}$, $H = (H_{jk})_{1\le j,k\le N}$ and $P = (P_{jk})_{1\le j,k\le N}$.

$$\begin{aligned} M_{jk} &= \begin{cases} \lambda_j^{N-k}\varphi_j, & k = odd; \\ \lambda_j^{N-k}\phi_j, & k = even. \end{cases} \\ H_{jk} &= \begin{cases} \lambda_j^{N}\phi_j, & k = 1; \\ \lambda_j^{N-k}\varphi_j, & k = even \ge 2; \\ \lambda_j^{N-k}\phi_j, & k = odd. \end{cases} \\ P_{jk} &= \begin{cases} \lambda_j^{N-k}\phi_j, & k = odd; \\ \lambda_j^{N-k}\varphi_j, & k = even. \end{cases} \end{aligned} \tag{2.11}$$

In order to study the new solutions of Eq. (1.3) by using the N-fold DT. First substituting the seed solution $q(x,t) = q(-x,-t) = 0$ into Lax pair (2.1) and (2.2), then the eigenfunction is solved as

$$\Psi_j = \begin{pmatrix} \phi_j \\ \varphi_j \end{pmatrix} = \begin{pmatrix} e^{i(\lambda_j^2 x + 2\lambda_j^4 t)} \\ e^{-i(\lambda_j^2 x + 2\lambda_j^4 t)} \end{pmatrix}. \tag{2.12}$$

Then we can construct important solutions for the reverse-space-time DNLS equation by substituting the eigenfunction Eq.(2.12) into N-fold DT formula (2.10).

Theorem 3. *Taking seed solution $q = 0$ in (2.10), then the solution $q[N]$=$-2i\sum_{j=1}^{N}\lambda_j$ at origin $(x,t) = (0,0)$.*

Proof. Taking seed solution $q = 0$, $x = 0$ and $t = 0$ in the following.

$$q[N](0,0) = 2i\frac{|M(0,0)H(0,0)|}{|P(0,0)^2|} = 2i\frac{|H(0,0)|}{|P(0,0)|} = -2i\sum_{j=1}^{N}\lambda_j. \tag{2.13}$$

So solution $q[N]$ derived by seed solution $q = 0$ at point (x,t)=$(0,0)$ is $-2i\sum_{j=1}^{N}\lambda_j$. □

N=1: the solution $q[1]$ with $\lambda_1 = \alpha_1 + i\beta_1$ is expressed as follows

$$\begin{aligned} q[1] &= (2i\alpha_1 - 2\beta_1)e^{iA+B}, \\ A &= -2(2\alpha_1^4 t - 12\alpha_1^2\beta_1^2 t + 2\beta_1^4 t + \alpha_1^2 x - \beta_1^2 x), \\ B &= 2(8\alpha_1^3\beta_1 t - 8\alpha_1\beta_1^3 t + 2\alpha_1\beta_1 x). \end{aligned} \tag{2.14}$$

When $\alpha_1\beta_1 = 0$, $|q[1]|^2 = 4(\alpha_1^2 + \beta_1^2)$, which is a plane wave with height of $2\sqrt{\alpha_1^2 + \beta_1^2}$.
When $\alpha_1\beta_1 \neq 0$, $|q[1]|^2 = 4(\alpha_1^2 + \beta_1^2)e^{8\alpha_1\beta_1(4\alpha_1^2 t - 4\beta_1^2 t + x)}$, which is an exponentially growing curved surface wave.

N=2: Let $\lambda_1 = \alpha_1 + i\beta_1$, $\lambda_2 = \alpha_2 + i\beta_2$, an explicit expression of $q[2]$ is as follows.

$$q[2] = \frac{2i\zeta_1 e^{iA_1} B[\zeta_1 B \sin A_4 \sin A_3 + \zeta_2 \sin(A_3 - A_4) + \zeta_1 \cos A_4 \cos A_3]}{[\zeta_2 \sin(A_3 - A_4) - \zeta_1 \cos(A_3 + A_4)]^2}, \tag{2.15}$$

where

$$\begin{aligned} B &= \cosh A_2 - \sinh A_2, \\ A_1 &= (2\alpha_1^4 - 12\alpha_1^2\beta_1^2 + 2\alpha_2^4 - 12\alpha_2^2\beta_2^2 + 2\beta_1^4 + 2\beta_2^4)t - (-\alpha_1^2 - \alpha_2^2 + \beta_1^2 + \beta_2^2)x, \\ A_2 &= (8\alpha_1^3\beta_1 - 8\alpha_1\beta_1^3 + 8\alpha_2^3\beta_2 - 8\alpha_2\beta_2^3)t + 2x(\alpha_1\beta_1 + \alpha_2\beta_2), \\ A_3 &= 2\alpha_2^4 t + 8i\alpha_2^3\beta_2 t + (-12\beta_2^2 t + x)\alpha_2^2 - 8i(\beta_2^2 t - \frac{1}{4}x)\beta_2\alpha_2 + 2\beta_2^4 t - \beta_2^2 x, \\ A_4 &= 2\alpha_1^4 t + 8i\alpha_1^3\beta_1 t + (-12\beta_1^2 t + x)\alpha_1^2 - 8i(\beta_1^2 t - \frac{1}{4}x)\beta_1\alpha_1 + 2\beta_1^4 t - \beta_1^2 x, \\ \zeta_1 &= \alpha_1 + i\beta_1 - \alpha_2 - i\beta_2, \quad \zeta_2 = i\alpha_1 + i\alpha_2 - \beta_1 - \beta_2. \end{aligned} \tag{2.16}$$

When $\alpha_2 = \alpha_1$, $\beta_2 = -\beta_1$ or $\alpha_2 = -\alpha_1$, $\beta_2 = \beta_1$, then $A_2 = 0$ and $A_3 + A_4 = 0$ in the Eq.(2.15). Now the soliton solution can be constructed. Namely, the soliton solution can be constructed by taking $\lambda_2 = \pm\lambda_1^* = \pm(\alpha_1 - i\beta_1)$. Without loss of generality, let $\lambda_2 = -\lambda_1^* = -\alpha_1 + i\beta_1$, then

$$q[2] = -2\zeta_1 e^{iH} \frac{\zeta_1 \cosh(F - iH) + i\zeta_2 \sinh(F - iH)}{(i\zeta_2 \sinh(F - iH) - m)^2}, \tag{2.17}$$

where

$$\begin{aligned} H &= 2(\alpha_1^2 - \beta_1^2)x + 4(\beta_1^4 - 6\alpha_1^2\beta_1^2 + \alpha_1^4)t), \\ F &= 16\alpha_1^3\beta_1 t - 16\alpha_1\beta_1^3 t + 4\alpha_1\beta_1 x. \end{aligned} \tag{2.18}$$

The center trajectory equation of solution $q[2]$ is calculated as $x = 4(\beta_1^2 - \alpha_1^2)t$ and the amplitude of $q[2]$ is $4|\beta_1|$. Furthermore, $q[2]$ become a rational soliton solution by the limit technique $\alpha_1 \to 0$,

$$q[2]_r = \frac{e^{2i\beta_1^2(2\beta_1^2 t - x)}(64it\beta_1^5 - 16ix\beta_1^3 - 4\beta_1)}{1 - 256\beta_1^8 t^2 + 128\beta_1^6 tx + (32it - 16x^2)\beta_1^4 - 8i\beta_1^2 x}, \tag{2.19}$$

where β_1 is an arbitrary real constant. From $|q[2]_r|^2 = \frac{16\beta_1^2}{(16\beta_1^4 t - 4\beta_1^2 x)^2 + 1}$, we know that $q[2]_r$ is an analytical solution at whole (x, t) plane and its trajectory is defined explicitly by $x = 4\beta_1^2 t$.

When $\alpha_1 = \alpha_2 = 0$ or $\beta_1 = \beta_2 = 0$ then $A_2 = 0$ in Eq.(2.15). It's mean $q[2]$ can represent periodic solutions when λ_1 and λ_2 are pure imaginary numbers or real numbers. For example $\lambda_1 = i\beta_1$, $\lambda_2 = i\beta_2$ and $\beta_1 \neq \pm\beta_2$ in the Eq.(2.15).

$$q[2] = 2i\zeta_1 e^{i(K_1 + K_2)} \frac{\zeta_1 \cos(K_1 - K_2) + \zeta_2 \sin(K_1 - K_2)}{[-\zeta_1 \cos(K_1 + K_2) + \zeta_2 \sin(K_1 - K_2)]^2}, \tag{2.20}$$

where $K_1 = 2\beta_2^2(2\beta_2^2 t - x)$ and $K_2 = 2\beta_1^2(2\beta_1^2 t - x)$.

The periodic of $q[2]$ is $\frac{\pi}{\beta_1^2 - \beta_2^2}$. The maximum and min amplitude of the periodic solution occurs at $x = 2(\beta_1^2 + \beta_2^2)t$ and $x = \frac{4\beta_1^4 t - 4\beta_2^4 t + \pi}{2\beta_1^2 - 2\beta_2^2}$, the maximum and min amplitude of the periodic solution $q[2]$ is $2(|\beta_1| + |\beta_2|)$ and $\frac{4(\beta_1+\beta_2)^2(\beta_1-\beta_2)^2 \mathrm{e}^{\frac{i\pi(\beta_1^2+\beta_2^2)}{(\beta_1-\beta_2)(\beta_1+\beta_2)}}}{\left(\mathrm{e}^{\frac{i\beta_2^2\pi}{(\beta_1-\beta_2)(\beta_1+\beta_2)}}\beta_1 - \mathrm{e}^{\frac{i\beta_1^2\pi}{(\beta_1-\beta_2)(\beta_1+\beta_2)}}\beta_2\right)\left(\beta_1 \mathrm{e}^{\frac{i\beta_1^2\pi}{(\beta_1-\beta_2)(\beta_1+\beta_2)}} - \mathrm{e}^{\frac{i\beta_2^2\pi}{(\beta_1-\beta_2)(\beta_1+\beta_2)}}\beta_2\right)}$. We can control the amplitude and period of the periodic solutions by adjusting parameter values β_1 and β_2. In particular, when $\beta_1 = -\beta_2$, the periodic solution degenerates into a plane wave solution.

Taking $\lambda_j = i\beta_j$, $j = 1, .., 2n$, $2n = N$, the n-periodic solutions can be constructed by N-fold DT formula (2.10) with zero seed solution.

Corollary 4. *The height of n-periodic wave solutions $q[N]$ is $2|\sum_{j=1}^{2n}\beta_j|, 2n = N$.*

In Fig.1, we give the dynamics plot of periodic, double-periodic and three-periodic solutions. We plot the one-periodic solution in Fig.1(a) by taking $\beta_1 = 1$, $\beta_2 = 0.5$. Intuitively, a one-periodic solution looks like a set of parallel solitons. Double-periodic solutions are two sets of parallel solitons with different directions. A peak is created at the location of the periodic waves collision, so the double-periodic dynamic evolution looks like a set of parallel peaks with equal amplitude (See Fig.1(b)). A linear superposition of amplitudes can be generated when the two periodic waves collisions and the amplitude of the double-periodic wave is $2(|\sum_{j=1}^{4}\beta_j|)$. Looking at the density diagram, we can see that the double-periodic waves occur phase shifts, which is very similar to the elastic collision of solitons.

The dynamic evolution diagram of n-periodic solution ($n > 2$) will show more complex structure, because the elastic collision of three periodic solutions with different directions and velocities, which will produce peaks with different amplitudes and size. Due to the frequent collision of periodic waves will result in the frequent phase shift, the density graph of n-periodic wave presents irregular curves (See Fig.1(c)).

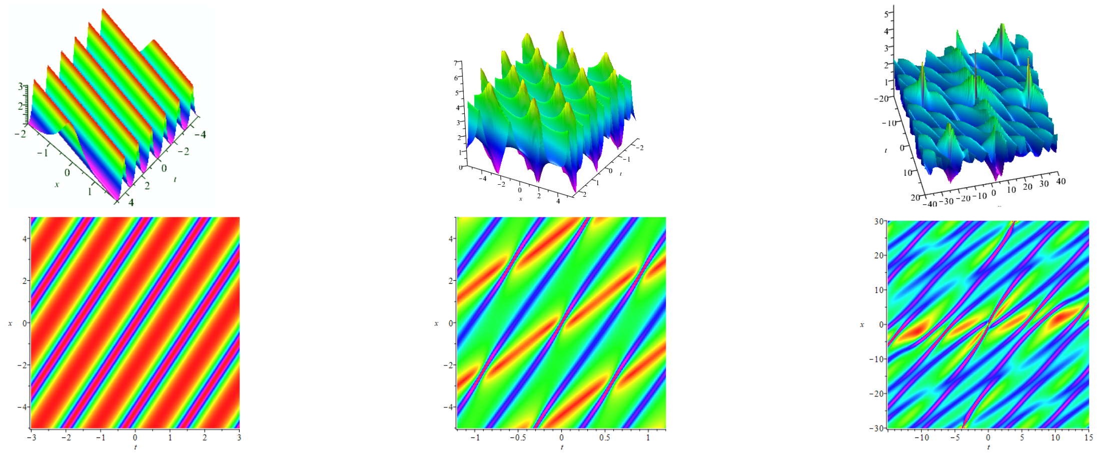

(a) (b) (c)

FIGURE 1. (a) Periodic solution: $\beta_1 = 1$, $\beta_2 = 0.5$; (b) Double-periodic solution: $\lambda_1 = i$, $\lambda_2 = 0.5i$, $\lambda_3 = 0.1i$, $\lambda_4 = \sqrt{2}i$; (c) Three-periodic solution: $\lambda_1 = 0.1i$, $\lambda_2 = 0.9i$, $\lambda_3 = 0.2i$, $\lambda_4 = 0.8i$, $\lambda_5 = 0.3i$, $\lambda_6 = 0.7i$;

In the Fig. 2, we construct n-periodic solutions with different periods of the same amplitude by controlling parameters and show the cross-section of n-periodic solution when $n = 1, 2, 3, 4$. From the cross-sectional view, when n is larger, the periodicity of the periodic wave is worse, and even the form of quasi rogue wave solution appears. The reason for this is that when n increases, it is rare for n single periodic waves to collide completely.In the figure below, we use different colors to represent n-periodic solutions with different parameters.

From the symmetry relation of DNLS equation and reverse-space-time DNLS equation, we know that when λ_k is pure imaginary number or $\lambda_k^* = -\lambda_l$, $k \neq l$. Solution (2.17) and solution (2.20) of reverse-space-time DNLS equation are also the solutions of DNLS equation. In the following, we will give the multi-soliton souliton, n-periodic solution and the mixed solution of reverse-space-time DNLS equation by the even-fold DT.

Taking $\lambda_{2k} = -\lambda_{2k-1}^* = -\alpha_{2k-1} + i\beta_{2k-1}$, $k = 1, ..n$, $n = \frac{N}{2}$. We can construct n-solitons solutions by N-fold DT.

Corollary 5. *The height of n-solitons solutions $q[N]$ is $4|\sum_{k=1}^{n}\beta_{2k-1}|, n = \frac{N}{2}$.*

When $\beta_{2k-1}^2 - \alpha_{2k-1}^2 \neq v_0$, the elastic collision n-solitons can be obtained. Otherwise, we can construct the velocity resonance n-solitons. Moreover, according to the center trajectory equation of the solution $q[n]$, the propagation direction and velocity of the soliton are affected by α_{2k-1} and β_{2k-1}. As an application, we show the elastic collision two-soliton, three-soliton and four-soliton in the Fig.3.

Also the velocity resonance of two-soliton, three-soliton and four-soliton are plot in Fig.4.

At the same time, The mixed solution of elastic collision solitons and velocity resonance solitons are plot in Fig. 5.

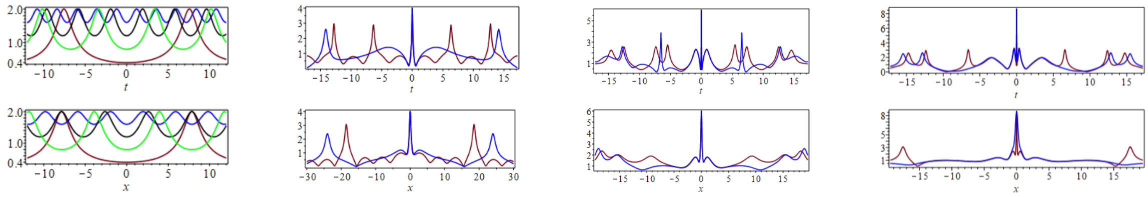

(a) (b) (c) (d)

FIGURE 2. Periodic solution (a) Blue:$\beta_1 = 0.1$, $\beta_2 = 0.9$; Black:$\beta_1 = 0.2$, $\beta_2 = 0.8$; Green:$\beta_1 = 0.3$, $\beta_2 = 0.7$; Red:$\beta_1 = 0.4$, $\beta_2 = 0.6$; Double-periodic solution (b) Blue:$\lambda_1 = 0.1i$, $\lambda_2 = 0.9i$, $\lambda_3 = 0.2i$, $\lambda_4 = 0.8i$; Red:$\lambda_1 = 0.1i$, $\lambda_2 = 0.9i$, $\lambda_3 = 0.2i$, $\lambda_4 = 0.8i$; Three-periodic solution (c) Blue:$\lambda_1 = 0.1i$, $\lambda_2 = 0.9i$, $\lambda_3 = 0.2i$, $\lambda_4 = 0.8i$, $\lambda_5 = 0.4i$, $\lambda_6 = 0.6i$; Red: $\lambda_1 = 0.1i$, $\lambda_2 = 0.9i$, $\lambda_3 = 0.2i$, $\lambda_4 = 0.8i$, $\lambda_5 = 0.3i$, $\lambda_6 = 0.7i$; Four-periodic solution (c) Blue: $\lambda_1 = 0.1i$, $\lambda_2 = 0.9i$, $\lambda_3 = 0.2i$, $\lambda_4 = 0.8i$, $\lambda_5 = 0.3i$, $\lambda_6 = 0.7i$, $\lambda_7 = 0.4i$, $\lambda_8 = 0.6i$; Red: $\lambda_1 = 0.15i$, $\lambda_2 = 0.85i$, $\lambda_3 = 0.2i$, $\lambda_4 = 0.8i$, $\lambda_5 = 0.3i$, $\lambda_6 = 0.7i$,$\lambda_7 = 0.4i$, $\lambda_8 = 0.6i$.

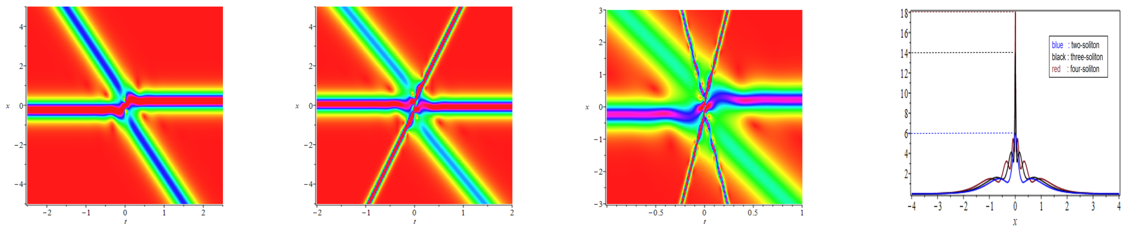

(a) (b) (c) (d)

FIGURE 3. (a) Two-soliton: $\lambda_1 = 1 + i$, $\lambda_2 = -1 + i$, $\lambda_3 = 1 + \frac{1}{2}i$, $\lambda_4 = -1 + \frac{1}{2}i$; (b) Three-soliton : $\lambda_1 = 1 + i$, $\lambda_2 = -1 + i$, $\lambda_3 = 1 + \frac{1}{2}i$, $\lambda_4 = -1 + \frac{1}{2}i$, $\lambda_5 = 1 + 2i$, $\lambda_6 = -1 + 2i$; (c) Four-soliton: $\lambda_1 = 1+i$, $\lambda_2 = -1+i$, $\lambda_3 = 1+2i$, $\lambda_4 = -1+2i$, $\lambda_5 = 1+\frac{1}{2}i$, $\lambda_6 = -1+\frac{1}{2}i$, $\lambda_7 = 2+i$, $\lambda_8 = -2+i$; (d)Cross section view of two-soliton, three-soliton and four-soliton.

We can get the n_1-soliton on the n-periodic background by letting $\lambda_{2k} = -\lambda^*_{2k-1} = -\alpha_{2k-1} + i\beta_{2k-1}$, $k = 1, .., n_1$. $\lambda_j = i\beta_j$, $j = 1, .., 2n$, $2(n_1 + n) = N$ in the N-fold DT.

Corollary 6. *The height of n_1-soliton on the n-periodic background is* $4|\sum_{k=1}^{n_1} \beta_{2k-1}| + 2|\sum_{j=1}^{2n} \beta_j|$, $2(n_1 + n) = N$.

As an example, we just give the case of $n = 1$ and 2. **n=1**, when $n_1 = 1$, one-soliton on the periodic background is constructed. We can see from Fig. 6 that the soliton looks very similar to the dynamic image of the breathers solution due to the interception of the periodic background wave. We can also control the period of the periodic background by adjusting the values of the spectral parameters. Fig. 6 is the soliton solution under different periodic background. We can also see that the local structure of soliton on the periodic-background has a single peak with two caves which is similar to the rogue waves. This gives us an idea to construct rogue wave solutions from zero seed solutions, but the feasibility remains to be proved.

Then, elastic collision of two solitons on periodic background is constructed by setting $n_1 = 2$ (see Fig. 7(a)). In particular, if $\beta^2_{2j-1} - \alpha^2_{2j-1}{=}v_0$ (v_0 is constant), $j = 1, 2$. Then the velocity resonance of two solitons on periodic-background is derived (see Fig. 7(b)).

When $n_1 = 3$, elastic collision of three-solitons on periodic background is constructed (see Fig. 8(a)). In particular, if $\beta^2_{2j-1} - \alpha^2_{2j-1}{=}v_0$, $j = 1, 2$ and v_0 is constant, the elastic collision of velocity resonance two-solitons and one-soliton on the periodic background is derived (see Fig. 8(b)).

n=2, one-soliton on the double-periodic background can be constructed by taking $n_1 = 1$. In order to see the structure of soliton solution on the double-periodic background more clearly, we give a local magnification in the right of Fig. 9.

Moreover, $n_1 = 2$, elastic collision of two-solitons on the double-periodic background can be constructed (see Fig. 10(a)). In particular, if $\beta^2_j - \alpha^2_j{=}v_0$ ($j = 1, 2$, v_0 is constant), then the velocity resonance of two-solitons on double-periodic background is derived (see Fig. 10(b)). The dynamic diagrams of these new solutions show very complex and interesting wave structures, which were first plotted in this investigation.

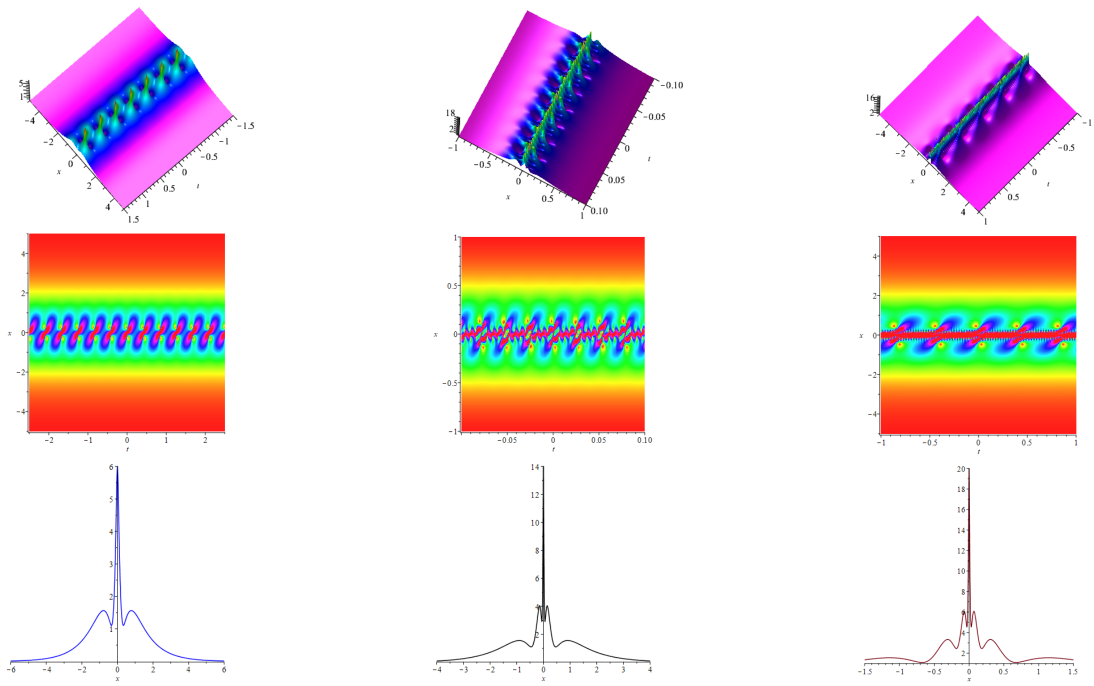

(a) (b) (c)

FIGURE 4. (a) Velocity resonance two-soliton: $\lambda_1 = 1+i$, $\lambda_2 = -1+i$, $\lambda_3 = \frac{1}{2}+\frac{1}{2}i$, $\lambda_4 = -\frac{1}{2}+\frac{1}{2}i$. (b) Velocity resonance three-soliton: $\lambda_1 = 1+i$, $\lambda_2 = -1+i$, $\lambda_3 = 2+2i$, $\lambda_4 = -2+2i$, $\lambda_5 = \frac{1}{2}+\frac{1}{2}i$, $\lambda_6 = -\frac{1}{2}+\frac{1}{2}i$; (c) Velocity resonance four-soliton solution: $\lambda_1 = 1+i$, $\lambda_2 = -1+i$, $\lambda_3 = \frac{1}{2}+\frac{1}{2}i$, $\lambda_4 = -\frac{1}{2}+\frac{1}{2}i$, $\lambda_5 = 2+2i$, $\lambda_6 = -2+2i$, $\lambda_7 = \frac{3}{2}+\frac{3}{2}i$, $\lambda_8 = -\frac{3}{2}+\frac{3}{2}i$.

3. Higher-order soliton on n-periodic background

When considering iterations of DT, the same seed cannot be used twice. How to generate higher-order soliton is an interesting problem, which must consider the nontrivial DT corresponding to $\lambda_j \to \lambda_1$, namely the degenerate Darboux transformation. To construct a n-periodic background, we also need to construct semi-degenerate DT in this section. The specific form of the degenerate/semi-degenerate DT is given as below.

Theorem 7. *Let* $\lambda_j \to \begin{cases} \lambda_1, & j = odd \le N-2\ell; \\ \lambda_2, & j = even \le N-2\ell. \end{cases}$, $\lambda_2 = -\lambda_1^* = -\alpha_1 + i\beta_1$. *Degenerate and semi-degenerate DT can be derived from N-fold DT formula* (2.10) *by Taylor expansion.*

$$q_N = \frac{|M'|^2}{|P'|^2} q + 2i\frac{|M'||H'|}{|P'|^2}. \tag{3.1}$$

Here

$$\begin{aligned} M' &= \begin{cases} M'_{jk}, & 1 \le j,k \le N-2\ell; \\ M_{jk}, & N-2\ell < j,k \le N. \end{cases} \\ H' &= \begin{cases} H'_{jk}, & 1 \le j,k \le N-2\ell; \\ H_{jk}, & N-2\ell < j,k \le N. \end{cases} \\ P' &= \begin{cases} P'_{jk}, & 1 \le j,k \le n-2\ell; \\ P_{jk}, & n-2\ell < j,k \le n. \end{cases} \end{aligned} \tag{3.2}$$

$$M'_{jk} = \lim_{\epsilon \to 0} \frac{\partial^{n_j-1} M'_{jk}(\lambda_j+\epsilon)}{(n_j-1)!\partial\epsilon^{n_j-1}},$$

$$H'_{jk} = \lim_{\epsilon \to 0} \frac{\partial^{n_j-1} H'_{jk}(\lambda_j+\epsilon)}{(n_j-1)!\partial\epsilon^{n_j-1}},$$

$$P'_{jk} = \lim_{\epsilon \to 0} \frac{\partial^{n_j-1} P'_{jk}(\lambda_j+\epsilon)}{(n_j-1)!\partial\epsilon^{n_j-1}},$$

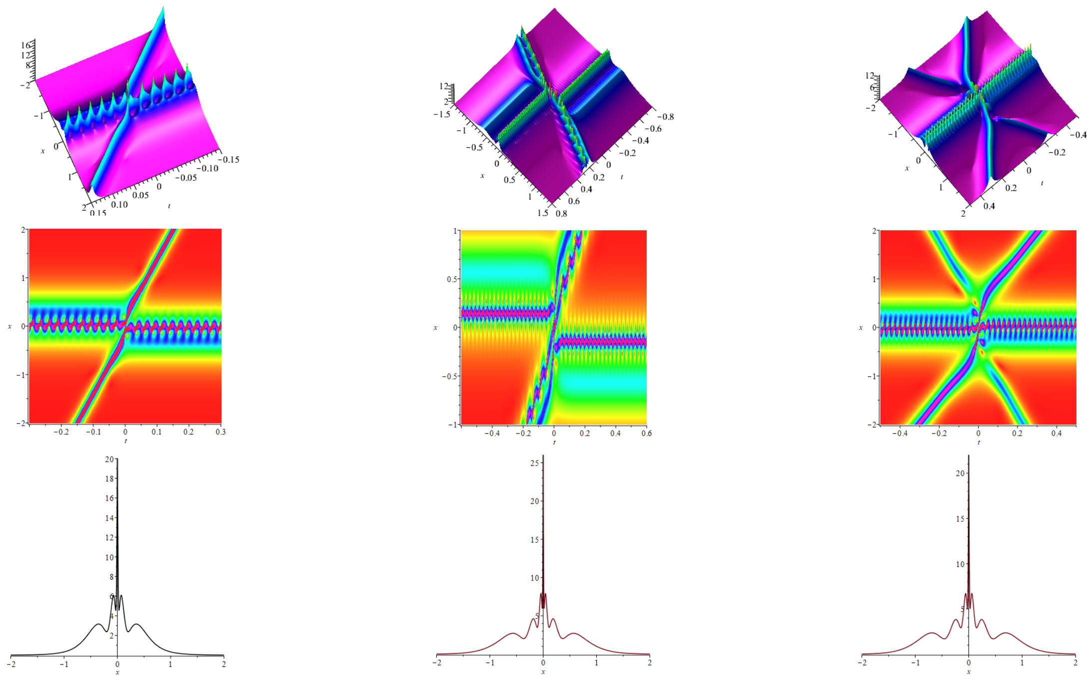

(a) (b) (c)

FIGURE 5. (a) Elastic collision of one-soliton and velocity resonance two-soliton: $\lambda_1 = 1+i$, $\lambda_2 = -1+i$, $\lambda_3 = 2+2i$, $\lambda_4 = -2+2i$, $\lambda_5 = 1+2i$, $\lambda_6 = -1+2i$. (b) Two velocity resonance two-soliton: $\lambda_1 = 1+i$, $\lambda_2 = -1+i$, $\lambda_3 = 2+2i$, $\lambda_4 = -2+2i$, $\lambda_5 = 1+\frac{3}{2}i$, $\lambda_6 = -1+\frac{3}{2}i$, $\lambda_7 = \frac{\sqrt{11}}{2}+2i$, $\lambda_8 = -\frac{\sqrt{11}}{2}+2i$; (c) Elastic collision of two-soliton and velocity resonance two-soliton: $\lambda_1 = 1+i$, $\lambda_2 = -1+i$, $\lambda_3 = 2+2i$, $\lambda_4 = -2+2i$, $\lambda_5 = 1+\frac{3}{2}i$, $\lambda_6 = -1+\frac{3}{2}i$, $\lambda_7 = \frac{\sqrt{11}}{2}+i$, $\lambda_8 = -\frac{\sqrt{11}}{2}+i$.

$$n_j = \left[\frac{j+1}{2}\right].$$

Proof. Starting from formula (2.10), let $\lambda_j \to \begin{cases} \lambda_1, & \text{j=odd;} \\ \lambda_2, & \text{j=even.} \end{cases}$. It's been stated in the article that only the case of N is even number is considered, so we can take $N = 2k$ at there.

Firstly, do the first order Taylor expansion in all the elements of the first and second row with respect to ε_1. Extract ε_1 in the first and second row, then take $\varepsilon_1 \to 0$;

Secondly, taking $\lambda_{2k-1-2\ell} = \lambda_1 + \varepsilon_{2k-1-2\ell}$, $\lambda_{2k-2\ell} = -\lambda_1 + \varepsilon_{2k-1-2\ell}$ and do the $k-\ell$-order Taylor expansion in all the elements of the $2k-1-2\ell$-th and $2k-2\ell$-th row with respect to $\varepsilon_{2k-1-2\ell}$. Subtract the first, third, ... , $(2k-3-2\ell)$-th row from the $(2k-1-2\ell)$-th row and subtract the second, fourth, ... , $(2k-2-2\ell)$-th row from the $2k-2\ell$-th row. Extract $\varepsilon_{2k-1-2\ell}^{k-1-\ell}$ in the $(2k-1-2\ell)$-th row and $(2k-2\ell)$-th row, then take $\varepsilon_{2k-1-2\ell} \to 0$, where $\varepsilon_{2k-1-2\ell}$ is the real constant ε_k;

Then, all the elements of the $(2k-2\ell+1)$-th to the $2k$-th row remain unchanged. Finally, the degenerate/semi-degenerate DT formula q_N can be derived through determinant calculation. □

Theorem 8. *The height of high-order solitons q_N derived by $\ell = 0$ in (3.1) is $N|\lambda_1+\lambda_2|$.*

Proof. Taking seed solution $q = 0$, then we can derive the following conclusion from (3.1)

$$q_N = 2i\frac{|M'H'|}{|P'^2|}. \tag{3.3}$$

We shall set $x = 0$ and $t = 0$ in a in following to study the height of high-order solitons q_N without the loss of the generality.

$$q_N(0,0) = 2i\frac{|M'(0,0)H'(0,0)|}{|P'(0,0)^2|} = 2i\frac{|H'(0,0)|}{|P'(0,0)|} = -iN(\lambda_1+\lambda_2). \tag{3.4}$$

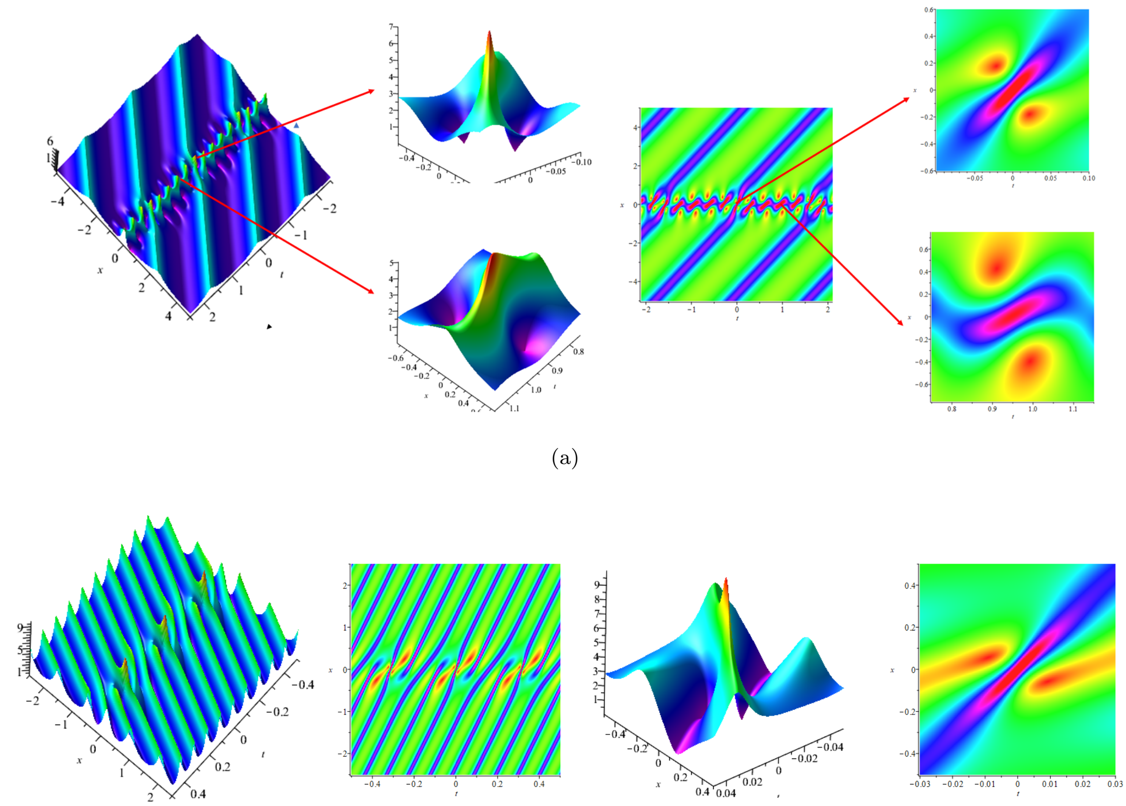

(a)

(b)

FIGURE 6. One soliton on the different periodic background (a): $\lambda_1 = 1+i$, $\lambda_2 = -1+i$, $\lambda_3 = i$, $\lambda_4 = \frac{1}{2}i$; (b) : $\lambda_1 = 1+i$, $\lambda_2 = -1+i$, $\lambda_3 = i$, $\lambda_4 = 2i$.

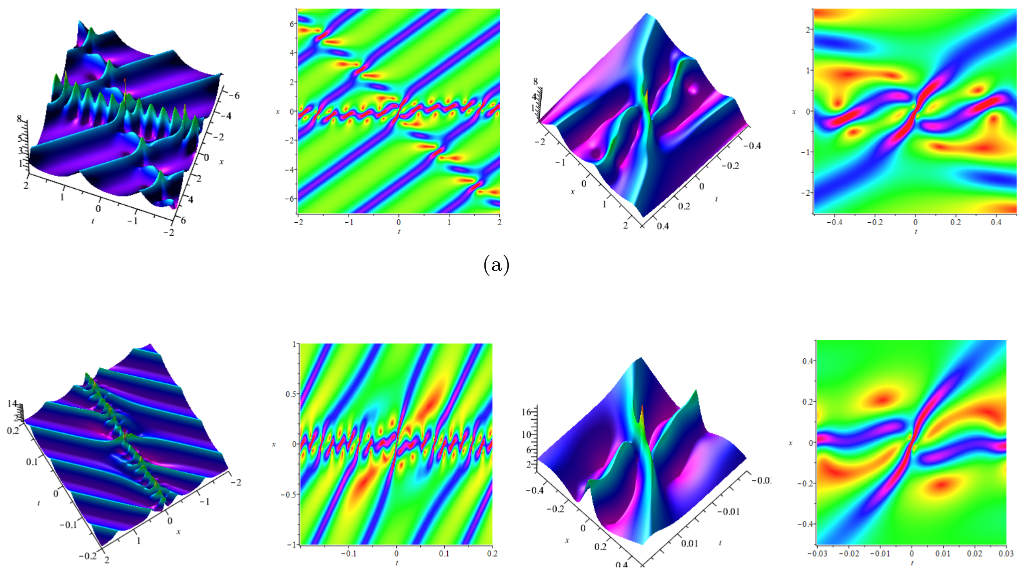

(a)

(b)

FIGURE 7. (a) Two soliton on periodic background: $\lambda_1 = 1+i$, $\lambda_2 = -1+i$, $\lambda_3 = 1+\frac{1}{2}i$, $\lambda_4 = -1+\frac{1}{2}i$, $\lambda_5 = i$, $\lambda_6 = \frac{1}{2}i$; (b) Velocity resonance two solitons on periodic periodic: $\lambda_1 = 1+i$, $\lambda_2 = -1+i$, $\lambda_3 = 2+2i$, $\lambda_4 = -2+2i$, $\lambda_5 = 2i$, $\lambda_6 = i$.

So the height of high-order solitons q_N in (3.1) is $N|\lambda_1 + \lambda_2|$. $\square$

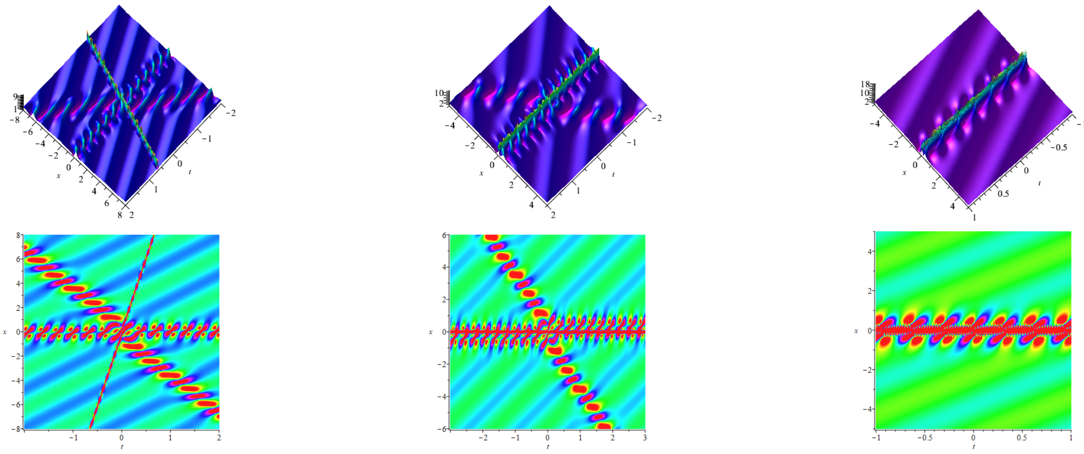

(a) (b) (c)

FIGURE 8. (a) Three soliton on the periodic background: $\lambda_1 = 1+i$, $\lambda_2 = -1+i$, $\lambda_3 = 1+2i$, $\lambda_4 = -1+2i$, $\lambda_5 = 1+\frac{1}{2}i$, $\lambda_6 = -1+\frac{1}{2}i$, $\lambda_7 = 0.1i$, $\lambda_8 = i$; (b) Elastic collision of velocity resonance two-soliton and one-soliton on the periodic background: $\lambda_1 = 1+i$, $\lambda_2 = -1+i$, $\lambda 3 = 2+2i$, $\lambda_4 = -2+2i$, $\lambda_5 = 1+\frac{1}{2}i$, $\lambda_6 = -1+\frac{1}{2}i$, $\lambda_7 = 0.1i$, $\lambda_8 = i$.

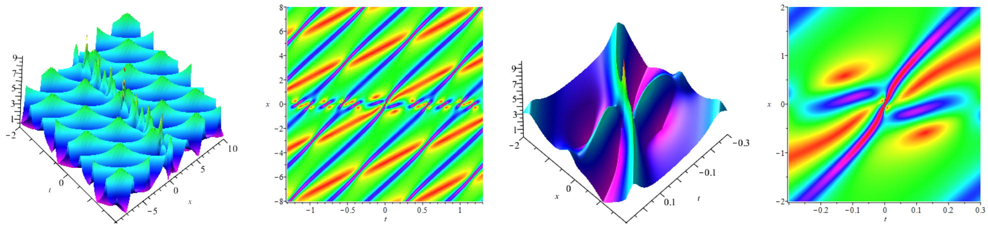

FIGURE 9. One-soliton on the double-periodic background: $\lambda_1 = 1+i$, $\lambda_2 = -1+i$, $\lambda_3 = i$, $\lambda_4 = \frac{1}{2}i$, $\lambda_5 = 0.1i$, $\lambda_6 = \sqrt{2}i$.

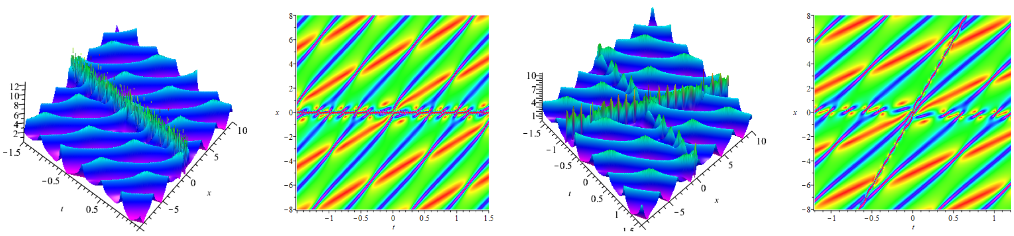

(a) (b)

FIGURE 10. (a) Velocity resonance two-soliton on the double-periodic background: $\lambda_1 = 1+i$, $\lambda_2 = -1+i$, $\lambda_3 = 2+2i$, $\lambda_4 = -2+2i$, $\lambda_5 = i$, $\lambda_6 = \frac{1}{2}i$, $\lambda_7 = 0.1i$, $\lambda_8 = \sqrt{2}i$; (b) Elastic collision two-soliton on the double-periodic background: $\lambda_1 = 1+i$, $\lambda_2 = -1+i$, $\lambda_3 = 1+2i$, $\lambda_4 = -1+2i$, $\lambda_5 = i$, $\lambda_6 = \frac{1}{2}i$, $\lambda_7 = 0.1i$, $\lambda_8 = \sqrt{2}i$.

The higher-order soliton, higher-order soliton on the n-periodic background can be derived as follows by the degenerate and semi-degenerate DT, respectively.

Taking $\ell = 0$ in Theorem 2, we can get degenerate DT. Then the higher-order soliton solution can be constructed by using the degenerate DT. For example, in Theorem 2 by setting $N = 4$, 6 and 8, following the Fig. (11) depicts the second, third and fourth-order solitons.

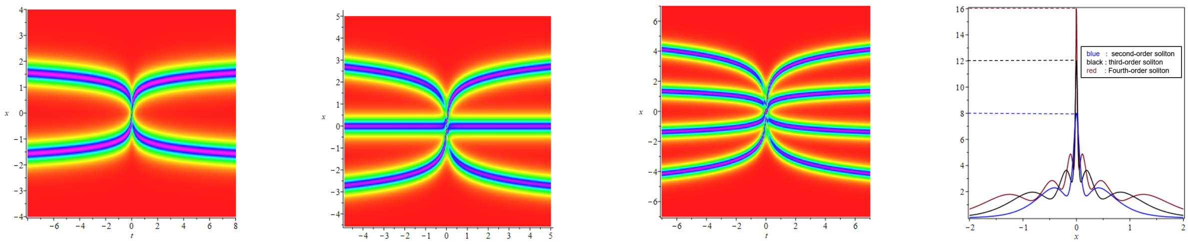

(a) (b) (c) (d)

FIGURE 11. (a) Second-order soliton: $\lambda_1 = 1+i, \lambda_2 = -1+i$; (b)Third-order soliton:$\lambda_1 = 1+i, \lambda_2 = -1+i$; (c) Fourth-order soliton: $\lambda_1 = 1+i, \lambda_2 = -1+i$; (d) Cross section view of second-order soliton, third-order soliton and fourth-order soliton.

By taking $\ell \neq 0$ in Theorem 2, the semi-degenerate DT is derived. The n-periodic solution can be obtained when taking $\ell \neq 0$ and all the spectral parameters which are not degenerated in the semi-degenerate DT as imaginary or real numbers. Since periodic solution and double-periodic solution can be constructed by 2-fold DT and 4-fold DT respectively, as an example, we only consider the case of $\ell = 1$ and $\ell = 2$ in this investigation.

Taking $\ell = 1$ in Theorem 2, the higher-order soliton on the periodic background can be constructed by the semi-degenerate DT formula. When $n = 6$, using the semi-degenerate DT 3.1, elastic collision of second-order soliton and one-soliton can be constructed by setting $\lambda_2 = -\lambda_1^* = -\alpha_1 + i\beta_1$, $\lambda_5 = \alpha_5 + i\beta_5$, $\lambda_6 = \alpha_6 + i\beta_6$ and $\alpha_5 \neq \alpha_6$ (see Fig.12(a)). In particular, when $\beta_5^2 - \alpha_5^2 = \beta_1^2 - \alpha_1^2$, velocity resonance of second-order soliton and one soliton is derived (see Fig.12(b)); when $\alpha_5 = \alpha_6 = 0$, the second-order soliton solution on the periodic background is constructed and the dynamic evolution diagram is plotted in Fig.12(c).

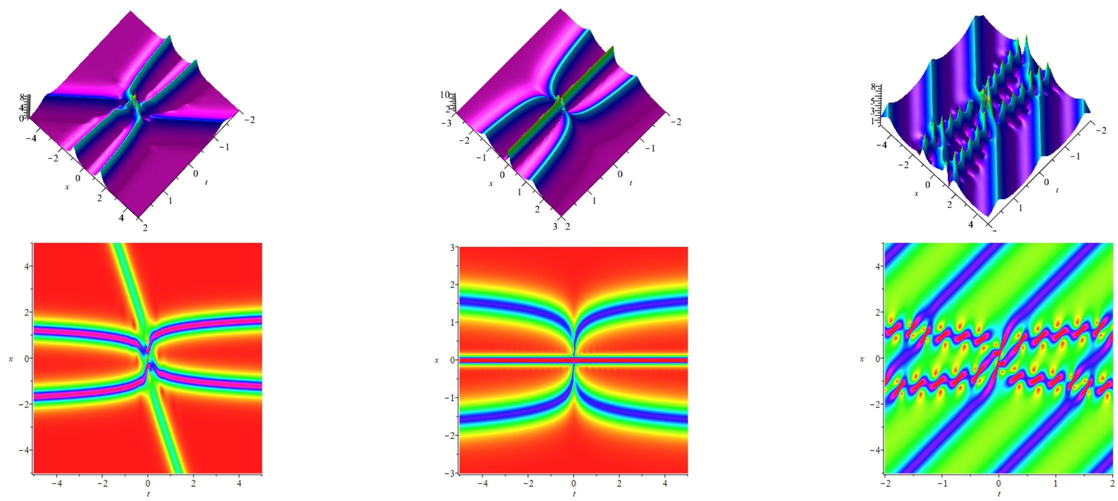

(a) (b) (c)

FIGURE 12. (a) Elastic collision of second-order soliton and one soliton: $\lambda_1 = 1+i, \lambda_2 = -1+i, \lambda_5 = 1+\frac{1}{2}i, \lambda_6 = -\frac{1}{2}i$; (b) Velocity resonance of second-order soliton and one soliton: $\lambda_1 = 1+i, \lambda_2 = -1+i, \lambda_5 = 2+2i, \lambda_6 = -2+2i$; (c) Second-order soliton solution on the periodic background: $\lambda_1 = 1+i, \lambda_2 = -1+i, \lambda_5 = i, \lambda_6 = \frac{1}{2}i$.

When $n = 8$, setting $\lambda_2 = -\lambda_1^* = -\alpha_1 + i\beta_1$, $\lambda_8 = -\lambda_7^* = -\alpha_7 + i\beta_7$, elastic collision of third-order soliton and one-soliton is constructed. In particular, velocity resonance of third-order soliton and one-soliton is constructed when $\beta_7^2 - \alpha_7^2 = \beta_1^2 - \alpha_1^2$. Third-order soliton on a periodic background is derived by setting $\lambda_2 = -\lambda_1^* = -\alpha_1 + i\beta_1$, $\lambda_7 = i\beta_7, \lambda_8 = i\beta_8$ and $\beta_7 \neq \pm\beta_8$. The dynamical evolution diagrams of these solutions can be seen in Fig.13(a), Fig.13(b) and Fig.13(c) respectively.

Taking $\ell = 2$, many interesting mixed solutions of higher-soliton, multi-soliton, periodic solution and double-periodic can be derived from $\lambda_2 = -\lambda_1^* = -\alpha_1 + i\beta_1$, $\lambda_{n-2} = -\lambda_{n-3}^* = -\alpha_{n-2} + i\beta_{n-2}$ and $\lambda_n = -\lambda_{n-1}^* = -\alpha_{n-1} + i\beta_{n-1}$.

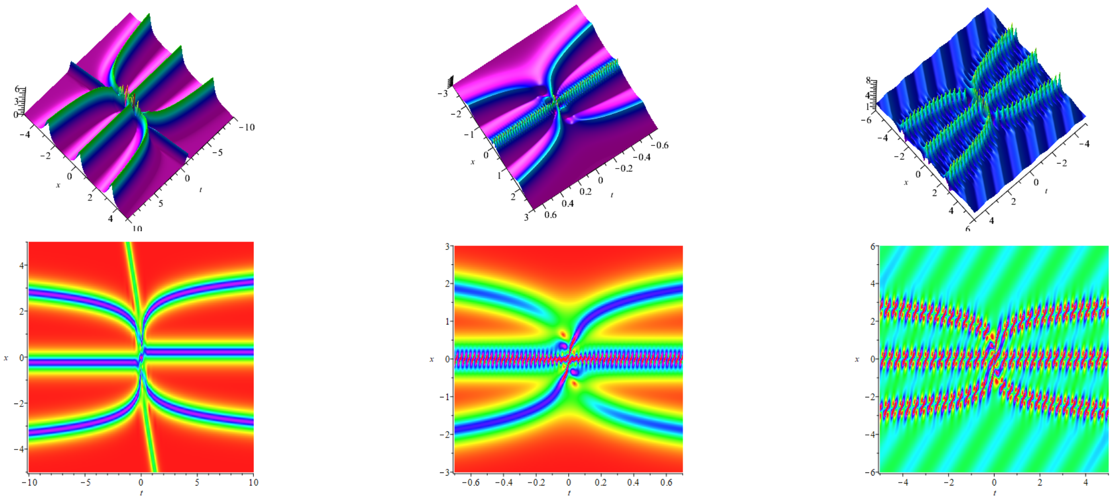

(a) (b) (c)

FIGURE 13. (a) Elastic collision of third-order soliton and one-soliton: $\lambda_1 = 1 + i, \lambda_2 = -1 + i, \lambda_7 = 1 + \frac{1}{2}i, \lambda_8 = -1 + \frac{1}{2}i$; (b) Velocity resonance of third-order soliton and one-soliton: $\lambda_1 = 1 + i, \lambda_2 = -1+i, \lambda_7 = 2+2i, \lambda_8 = -2+2i$; (c) Third-order soliton on the periodic background: $\lambda_1 = 1+i, \lambda_2 = -1 + i, \lambda_7 = 0.1i, \lambda_8 = i$.

Let us take $n = 8$ as an example, elastic collision of second-order soliton and two-soliton is constructed immediately by using the semi-degenerate DT formula 3.1, see the dynamic evolution diagram in Fig. 14(a). In particular, elastic collision of second-order soliton and velocity resonance two-soliton is derived when $\beta_5^2 - \alpha_5^2 = \beta_7^2 - \alpha_7^2$ (see Fig. 14(b)); Velocity resonance of second-order soliton and two-soliton is constructed when $\beta_1^2 - \alpha_1^2 = \beta_5^2 - \alpha_5^2 = \beta_7^2 - \alpha_7^2$ (see Fig. 14(c)).

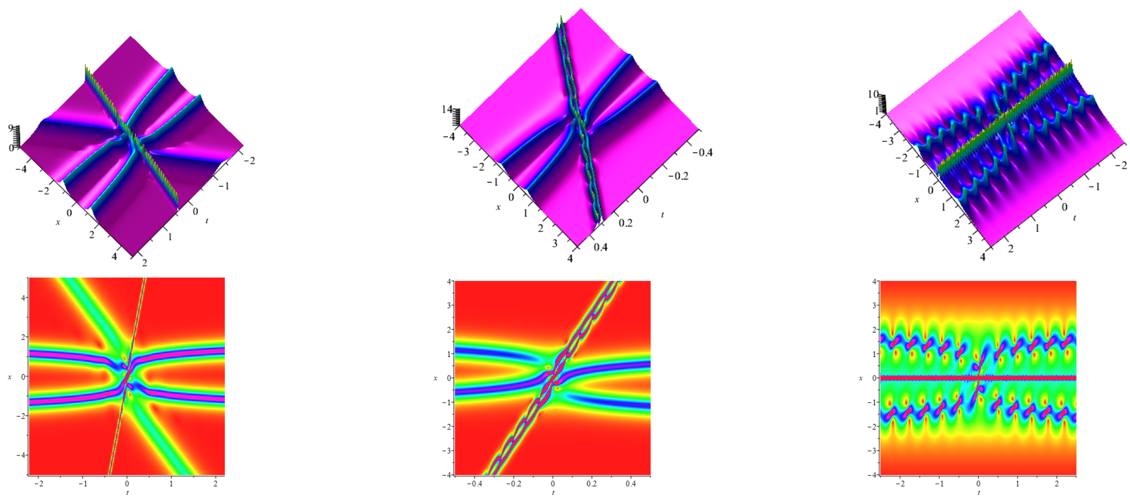

(a) (b) (c)

FIGURE 14. (a) Elastic collision of second-order soliton and two-soliton: $\lambda_1 = 1+i, \lambda_2 = -1+i, \lambda_5 = 1+\frac{1}{2}i, \lambda_6 = -1+\frac{1}{2}i, \lambda_7 = 1+2i, \lambda_8 = -1+2i$; (b) Elastic collision of second-order soliton and velocity resonance two-soliton: $\lambda_1 = 1+i, \lambda_2 = -1+i, \lambda_5 = 1+2i, \lambda_6 = -1+2i, \lambda_7 = \sqrt{2}+i\sqrt{5}, \lambda_8 = -\sqrt{2}+i\sqrt{5}$; (c) Velocity resonance of second-order soliton and two-soliton: $\lambda_1 = 1+i, \lambda_2 = -1+i, \lambda_5 = \frac{1}{2}+\frac{1}{2}i, \lambda_6 = -\frac{1}{2} + \frac{1}{2}i, \lambda_7 = 2 + 2i, \lambda_8 = -2 + 2i$.

Elastic collision of second-order soliton and one-soliton on the periodic can be derived by $\lambda_2 = -\lambda_1^* = -\alpha_1 + i\beta_1$, $\lambda_6 = -\lambda_5^* = -\alpha_5 + i\beta_5$ $\lambda_7 = i\beta_7, \lambda_8 = i\beta_8$. In particular, when $\beta_5^2 - \alpha_5^2 = \beta_1^2 - \alpha_1^2$ the velocity resonance of second-order soliton and one-soliton on the periodic background can be derived. When $\lambda_2 = -\lambda_1^* = -\alpha_1 + i\beta_1$, $\lambda_k = i\beta_k$, with $k = 5, 6, 7, 8$ are pure imaginary numbers, we can construct the second-order soliton on the double-periodic background. The dynamical evolution diagrams of these higher-order soliton on the periodic and double-periodic background are plotted in Fig.15(a), Fig.15(b) and Fig.15(c) respectively. From these figures we can know intuitively that the direction and position of the propagation of solitons along the periodic background have great influence on the morphology of solitons.

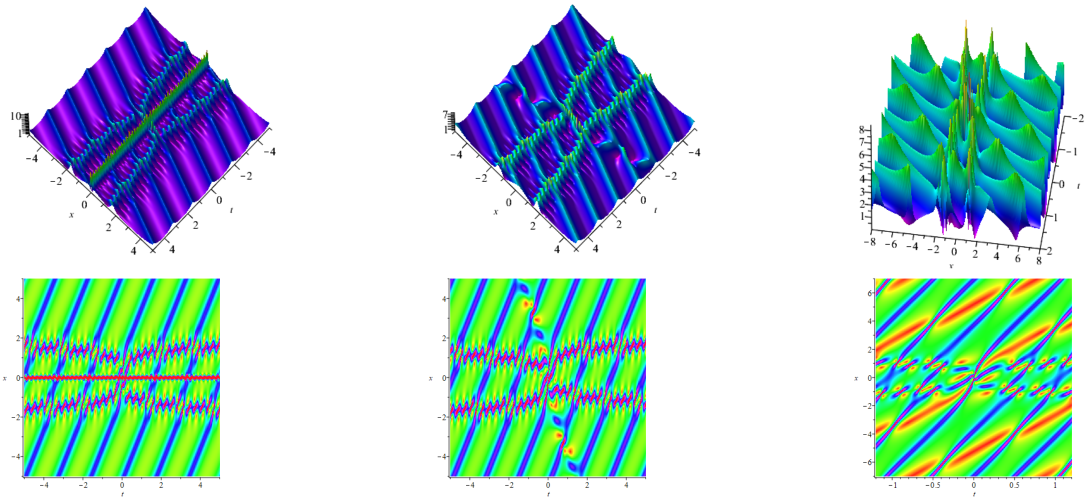

(a) (b) (c)

FIGURE 15. (a) Elastic collision of second-order soliton and one soliton on the periodic: $\lambda_1 = 1 + i, \lambda_2 = -1+i, \lambda_5 = 1+\frac{1}{2}i, \lambda_6 = -1+\frac{1}{2}i, \lambda_7 = i, \lambda_8 = \frac{1}{2}i$; (b) Velocity resonance of second-order soliton and one-soliton on the periodic background: $\lambda_1 = 1 + i, \lambda_2 = -1 + i, \lambda_5 = 2 + 2i, \lambda_6 = -2 + 2i, \lambda_7 = i, \lambda_8 = \frac{1}{2}i$; (c) Second-order soliton on the double-periodic background: $\lambda_1 = 1 + i, \lambda_2 = -1 + i, \lambda_5 = 0.1i, \lambda_6 = \sqrt{2}i, \lambda_7 = i, \lambda_8 = \frac{1}{2}i$.

4. HIGH-ORDER HYBRID-PATTERN SOLITONS ON THE n-PERIODIC BACKGROUND

In the previous section, we have investigated solution dynamics in the high-order one-soliton on the periodic and double periodic background. It is shown that the high-order one-soliton is moving on several different trajectories in nearly equal velocities. The high-order hybrid-pattern solitons describe the nonlinear interaction between several types of solitons, which gives rise to new types of high-order solitons with interesting dynamical patterns. It is also shown that high-order hybrid-pattern solitons could have more complicated wave structures and behave very differently from high-order one-solitons. In this section, we will study the high-order hybrid-pattern solitons on the n-periodic background by generalized degenerated DT and generalized semi-degenerated DT.

Theorem 9. *Setting*

$$\lambda_j \to \begin{cases} \lambda_1, & j = odd \le 2n_0 + 2n_1 - 1; \\ \lambda_2, & j = even \le 2n_0 + 2n_1; \\ \lambda_3, & 2n_0 + 2n_1 < j = odd \le 2n_0 + 2n_1 + 2n_2 - 1; \\ \lambda_4, & 2n_0 + 2n_1 < j = even \le 2n_0 + 2n_1 + 2n_2; \\ ... & \\ \lambda_{2n_0-1}, & 2n_0 + 2n_1 + ...2n_{\hbar-1} < j = odd \le 2n_0 + 2n_1 + ...2n_{\hbar-1} + 2n_\hbar - 1; \\ \lambda_{2n_0}, & 2n_0 + 2n_1 + ...2n_{\hbar-1} < j = even \le 2n_0 + 2n_1 + ...2n_{\hbar-1} + 2n_\hbar. \end{cases}$$

$$2\sum_{\ell=0}^{\hbar} n_\ell = N - 2s.$$

Generalized degenerated DT and generalized semi-degenerated DT can be derived from N-fold DT formula (2.10) *by Taylor expansion and determinant calculation. The specific form of the new solution q_N is as follows*

$$q_N = \frac{|M'|^2}{|P'|^2} q + 2i \frac{|M'||H'|}{|P'|^2}. \tag{4.1}$$

Here

$$
\begin{aligned}
M' &= \begin{cases} M'_{jk}, & 1 \le j,k \le N-2s; \\ M_{jk}, & N-2s < j,k \le N. \end{cases} \\
H' &= \begin{cases} H'_{jk}, & 1 \le j,k \le N-2s; \\ H_{jk}, & N-2s < j,k \le N. \end{cases} \\
P' &= \begin{cases} P'_{jk}, & 1 \le j,k \le N-2s; \\ P_{jk}, & N-2s < j,k \le N. \end{cases}
\end{aligned}
\tag{4.2}
$$

$$M'_{jk} = \lim_{\epsilon\to 0} \frac{\partial^{n_j} M'_{jk}(\lambda_j+\epsilon)}{n_j!\partial\epsilon^{n_j-1}},$$

$$H'_{jk} = \lim_{\epsilon\to 0} \frac{\partial^{n_j} H'_{jk}(\lambda_j+\epsilon)}{n_j!\partial\epsilon^{n_j-1}},$$

$$P'_{jk} = \lim_{\epsilon\to 0} \frac{\partial^{n_j} P'_{jk}(\lambda_j+\epsilon)}{n_j!\partial\epsilon^{n_j-1}},$$

$$
n_j = \begin{cases}
0, & j \le 2n_0; \\
\left[\frac{j-2n_0+1}{2}\right], & 2n_0 < j \le 2n_0+2n_1; \\
\left[\frac{j-2n_0-2n_1+1}{2}\right], & 2n_0+2n_1 < j \le 2n_0+2n_1+2n_2; \\
\ldots & \\
\left[\frac{j-2n_0-2n_1-\ldots-2n_{\hbar-1}+1}{2}\right], & 2n_0+2n_1+\ldots+2n_{\hbar-1} < j \le 2n_0+2n_1+\ldots+2n_{\hbar}.
\end{cases}
$$

The proof process of Theorem 3 is similar to those that were already presented in the proof of Theorem 2, so we choose to omit the details of our proof of Theorem 3.

When $s=0$, the generalized degenerated DT formula can be derived from Theorem 3. Taking $n=8$, elastic collision of two second-order soliton can be derived by $\lambda_2 = -\lambda_1^* = -\alpha_1 + i\beta_1$, $\lambda_4 = -\lambda_3^* = -\alpha_3 + i\beta_3$. It is shown that the two second-order solitons are moving on different trajectories in different velocities and amplitudes (see Fig.16(a)). In particular, elastic collision of two velocity resonance second-order solitons can be derived when $\beta_3^2 - \alpha_3^2 = \beta_1^2 - \alpha_1^2$. In Fig.16(b) and Fig.16(c), we give two different models of elastic collision of two velocity resonance second-order solitons depending on the choices of the parameters.

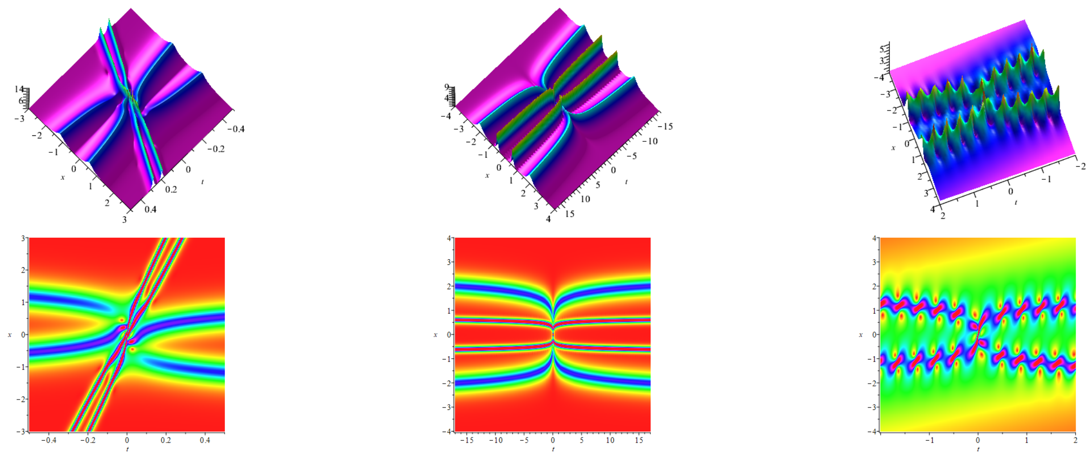

(a) (b) (c)

FIGURE 16. (a) Elastic collision of two second-order solitons : $\lambda_1 = 1+i, \lambda_2 = -1+i, \lambda_3 = 1+2i, \lambda_4 = -1+2i$; (b) Elastic collision of two velocity resonance second-order solitons : $\lambda_1 = 1+i, \lambda_2 = -1+i, \lambda_3 = 2+2i, \lambda_4 = -2+2i$; (c) Elastic collision of two second-order velocity resonance solitons : $\lambda_1 = 0.1+0.1i, \lambda_2 = -0.1+0.1i, \lambda_3 = 0.2+0.2i, \lambda_4 = -0.2+0.2i$.

Similar to the previous section, when $s = n$, we can consider the n-periodic solution. As a example, we just give the detail construction process for the case of $s = 1$ in this section. When $s = 1$, by using the generalized semi-degenerate DT, higher-order hybrid-pattern solution on the periodic and double-periodic background can be constructed. For example, when $N = 10$, the elastic collision of two second-order soliton on the periodic background is constructed by setting $\lambda_2 = -\lambda_1^* = -\alpha_1 + i\beta_1$, $\lambda_4 = -\lambda_3^* = -\alpha_3 + i\beta_3$, $\lambda_9 = i\beta_9$, $\lambda_{10} = i\beta_{10}$ (see Fig.17(a)). In particular, when $\beta_3^2 - \alpha_3^2 = \beta_1^2 - \alpha_1^2$, velocity resonance of two second-order solitons on the periodic background can be derived. As can be seen from the dynamic evolution diagram of solutions in Fig.17(c), high-order solitons with different velocities and directions show completely different soliton morphology under the influence of periodic background, and the periodic background will gradually weaken as time goes by, which is also consistent with the wave phenomenon in nature. Fig.17(b) is the local structure diagram of Fig.17(c), Fig.17(d) gives a different model for velocity resonance of two second-order solitons on the periodic background. The reason for this phenomenon is that the propagation pattern of solitons change greatly with the difference period of periodic background depending on the choices of the parameters.

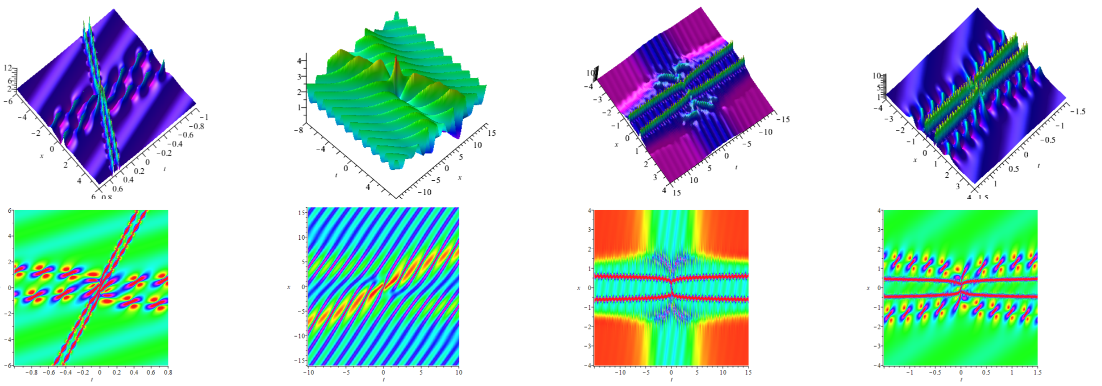

(a) (b) (c) (d)

FIGURE 17. (a) Elastic collision of two second-order solitons on the periodic background: $\lambda_1 = 1 + i, \lambda_2 = -1 + i, \lambda_3 = 1 + 2i, \lambda_4 = -1 + 2i, \lambda_9 = 0.1i, \lambda_{10} = i$; (b) Velocity resonance of two second-order solitons on the periodic background: $\lambda_1 = 0.1 + 0.1i, \lambda_2 = -0.1 + 0.1i, \lambda_3 = 0.2 + 0.2i, \lambda_4 = -0.2 + 0.2i, \lambda_9 = 0.1i, \lambda_{10} = i$; (c) and (d) Velocity resonance of two second-order soliton on the periodic background: $\lambda_1 = 1 + i, \lambda_2 = -1 + i, \lambda_3 = 2 + 2i, \lambda_4 = -2 + 2i, \lambda_9 = 0.1i, \lambda_{10} = i$.

When $s = n$, the high-order hybrid-pattern solitons on the n-periodic background can be derived by using the generalized semi-degenerate DT 11 also. For example, we can construct two second-order soliton solitons on the double-periodic background by taking $N = 12$ and $n = 2$, which requires determinant operation of order 12×12.

5. Modulational instability

Putting plane wave seed solution $q_0(x, t) = ce^{i(kx+wt)}$ into the Eq. (1.3), we obtain that $w = -c^2k + k^2$. Here c is amplitude, k is wave number and w is the background frequency. According to the MI theory, the perturbation solution can be derived as $q_1(x, t) = (c + P)e^{i(kx+wt)}$ by putting a small perturbation $P = m\exp(i(Kx + \Omega t)) + n\exp(-i(Kx + \Omega t))$ into plane wave seed solution $q_0(x, t)$. The K indicates the disturbance wave number and Ω indicates the disturbance frequency. Substituting the perturbation solution $q_1(x, t)$ into the Eq. (1.3), it can generate a system of linear homogeneous equations for the small parameters m and n as follows.

$$\begin{aligned} ((k + 2K)c^2 + (-K^2 - 2kK + \Omega))m + (k + K)c^2 n = 0,\\ (k - K)c^2 m + ((k - 2K)c^2 + 2kK - K^2 - \Omega)n = 0. \end{aligned} \tag{5.1}$$

It gives rise to the following dispersion relation equation

$$\Omega = (-2c^2 + 2k \pm \sqrt{c^4 - 2c^2k + K^2})K. \tag{5.2}$$

It can be conclude that the MI depends on the values of the amplitude c, wave number k and perturbation wave number K. Due to the above dispersion relation, we can see that when $c^4 - 2c^2k + K^2 \geq 0$, the time-dependent frequency Ω is real at any value of the wave number K, whereas Ω becomes complex and disturbance will grow with time exponentially. Let us consider the gain spectrum of MI. The power gain is obtained from

$$G(K) = Im(\Omega) = Im(|K|\sqrt{c^4 - 2c^2k + K^2}),$$

$G(K)$ represents the MI gain when $c^4 - 2c^2k + K^2 < 0$. The frequency Ω will exist the imaginary part which makes the perturbation function P exponentially increase and destroys the stability of the system. This instability is a condition for the existence of rogue wave. From the above analysis, it appears that there exists two distinctive MI and modulation stability (MS) regions, which are distinguished with each other clearly. In the region $c^4 - 2c^2k + K^2 < 0$, MI exists. On the contrary, if $c^4 - 2c^2k + K^2 \geq 0$, there appears MS region.

Let $c = 1$, we know the MI arises at $k > 0.5$. Fig. 18(a) gives the gain at the three different plane-wave numbers k and Fig. 18(b) gives the gain function. Because the gain function $G(K)$ is an even function $(G(K) = G(-K))$ about perturbation wave number K, So we can see the MI figure is symmetric about the line $K = 0$.

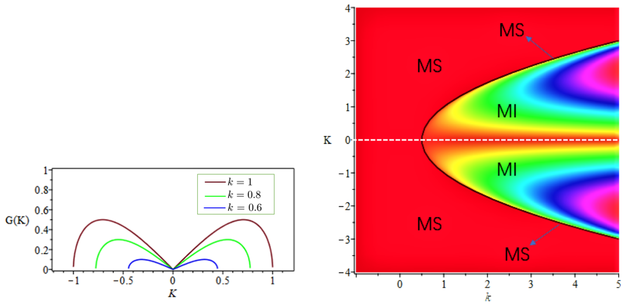

(a) (b)

FIGURE 18. (a) Gain at the three different plane-wave numbers k; (b) Gain function.

6. CONCLUSION

In this investigation, the N-fold DT, degenerate DT, semi-degenerate DT, generalized degenerate and semi-degenerate DT formulae for the reverse-space-time DNLS equation were presented by using concise expressions. The n-solitons solutions can be constructed by N-fold DT when taking $\lambda_{2k} = \pm\lambda^*_{2k-1} = \pm\alpha_{2k-1} \mp i\beta_{2k-1}$, $k = 1, ..n$, $2n = N$. The velocity resonance soliton is derived by $\beta_k^2 - \alpha_k^2 = v_0$ (v_0 is constant). When spectrum parameters λ_k are pure imaginary numbers or real numbers, the n-periodic solutions were constructed by the even-fold DT. When taking $\lambda_{2k} = -\lambda^*_{2k-1}$ or λ_k are pure imaginary numbers, the solutions satisfy both DNLS and reverse-space-time DNLS equation. In addition, the higher-order solitons, higher-order solitons on the n-periodic background, higher-order hybrid-pattern solitons and higher-order hybrid-pattern solitons on the n-periodic background were provided by degenerate DT, semi-degenerate DT, generalized degenerate DT and generalized semi-degenerate DT, separately.

Then giving a zero seed solution, the solution $q[N]$ obtained by N-fold DT at origin is equal to $-2i\sum_{j=1}^{N}\lambda_j$, which depends only on the spectral parameters. Also, we gave the corollary of the amplitude height of n-periodic wave solutions, m-soliton on the n-periodic background and high-order solitons is $2|\sum_{j=1}^{2n}\beta_j|, 2n = N$. $4|\sum_{k=1}^{m}\beta_{2k-1}| + 2|\sum_{j=1}^{2n}\beta_j|$, $2(m+n) = N$. and $N|\lambda_1 + \lambda_2|$, separately.

This is the first time to construct n-periodic solutions with zero seed solution. Intuitively, a periodic solution looks like a set of parallel solitons, double-periodic wave looks like parallel breathers. For the density figure of double-periodic waves which is very similar to the elastic collision of two sets of parallel solitons. The dynamic evolution diagram of n-periodic solution ($n > 2$) will show more complex structure, because the elastic collision of n-periodic solutions with different directions and velocities, which will produce peaks with different amplitudes and size. Due to the frequent collision of periodic waves will result in the frequent phase shift, the density figure of n-periodic wave presents irregular curves.

The dynamics of soliton on the periodic background show that the soliton looks very similar to the dynamic image of the breathers solution due to the interception of the periodic background. The period of the periodic background is controlled by adjusting spectral parameters. We found that the local structure of soliton on the periodic-background has a single peak with two caves which is similar to the rogue wave, which gives us an idea to construct rogue wave solutions from zero seed solutions, but the feasibility remains to be proved. In particular, the periodic solutions and solitons can be transformed into zero solution when $\sum_{j=1}^{N}\lambda_j = 0$.

It is shown that the high-order one-soliton is moving on several different trajectories in nearly equal velocities. Furthermore, the higher-order hybrid-pattern solitons describe the nonlinear interaction between several types of solitons, which gives rise to new types of high-order solitons with interesting dynamical patterns. When we put the perturbation of n-periodic background to the higher-order soliton and higher-order hybrid-pattern solitons, many interesting new phenomena emerge. It is also shown that high-order hybrid-pattern solitons have more complicated wave structures and behave very differently from high-order one-solitons. Interesting, these results also apply to the DNLS equation.

Finally, the conditions of generating MI and MS regions for the reverse-space-time DNLS equation were studied by MI analysis. These results would also be useful for understanding the corresponding soliton phenomena in many fields of local and nonlocal nonlinear dynamical systems such as ocean, nonlinear optics, Bose-Einstein condensates and other relevant fields.

References

[1] Kaup, D. J., Newell, A. C.: An exact solution for a derivative nonlinear Schrödinger equation. J. Math. Phys. **19**(4), 798-801 (1978)
[2] Zeng, Y.: New factorization of the Kaup-Newell hierarchy, Physica D. **73**, 171-188 (1994)
[3] Zhou, Z.X.: Parameters of darboux transformation for reduced akns, kaup-newell and pcf systems, Chinese Ann. Math. B **20**, 195-204 (1999)
[4] Imai, K. J.: Generlization of Kaup-Newell Inverse Scattering Formulation and Darboux Transformation, J.Phys.Soc.Japan. **68**, 355-359 (1999)
[5] Ma, W.X., Zhou, R.: A coupled AKNS-Kaup-Newell soliton hierarchy, J. Math. Phys. **40**(9), 4419-4428 (1999)
[6] Kundu, A.: Two-fold integrable hierarchy of nonholonomic deformation of the derivative nonlinear Schrödinger and the Lenells-Fokas equation, J. Math. Phys. **51**, 022901 (2010)
[7] Xu, S.W., He, J.S., Wang, L.H.: The Darboux transformation of the derivative nonlinear Schrödinger equation, J. Phys. A-Math. Theor. **44**, 6629-6636 (2011)
[8] Zhang, Y.S., Guo, L.J., Xu, S.W., Wu, Z.W., He, J.S.: The hierarchy of higher order solutions of the derivative nonlinear Schrödinger equation, Commun. Nonlinear Sci. **19**, 1706-1722 (2014)
[9] Xu, T., Chen, Y.: Mixed interactions of localized waves in the three-component coupled derivative nonlinear Schrödinger equations, Nonlinear Dyn. **92**, 2133-2142 (2018)
[10] Mjϕlhus, E.: On the modulational instability of hydromagnetic waves parallel to the magnetic field, J. Plasma Phys. **16**, 321-334 (1976)
[11] Lakhina, G.S., Sharma, A.S., Buchner, J.: International workshops on nonlinear waves and chaos in space plasmas-preface, Nonlinear Proc. Geoph. **11**(2), 181-181 (2004)
[12] Chen, X.J., Lam, W.K.: Inverse scattering transform for the derivative nonlinear Schrödinger equation with nonvanishing boundary conditions. Phys. Rev. E **69**, 066604 (2004)
[13] Spatchek, K.H., Shukla, P.K., Yu, M.Y.: Filamentation of lower-hybrid cones. Nucl. Fus. **18**, 290-293 (1977)
[14] Ichikawa, Y., Konno, K.. Wadati, M., Sanuki, H.: Spiky soliton in circular polarized Alfvén wave. J. Phys. Soc. Jpn. **48**, 279-286 (1980)
[15] Ruderman, M.S.: DNLS equation for large-amplitude solitons propagating in an arbitrary direction in a high-β hall plasma, J. Plasma Phys. **67**, 271-276 (2002)
[16] Shan, S.A., El-Tantawy, S.A.: The impact of positrons beam on the propagation of super freak waves in electron-positron-ion plasmas, Phys. Plasmas **23**(7), 072112 (2016)
[17] Tzoar, N., Jain, M.: Self-phase modulation in long-geometry optical waveguide, Phys. Rev. A **23**, 1266-1270 (1981)
[18] Anderson, D., Lisak, M.: Nonlinear asymmetric self-phase modulation and self-steepening of pulses in long Optical Waveguides, Phys. Rev. A **27**, 1393-1398 (1983)
[19] Govind, P.A.: Nonlinear fibers optics 3rd edn, New York: Adademic (2001)
[20] Ablowitz, M.J., Feng, B.F., Luo, X.D., Musslimani, Z.H.: Inverse scattering transform for the nonlocal reverse space-time nonlinear Schrödinger equation, Theor. Math. Phys. **196**, 1241-1267 (2018)
[21] Yang, J.K.: General N-solitons and their dynamics in several nonlocal nonlinear Schrödinger equations, Phys. Lett. A **383**(4), 328-337 (2019)
[22] Wang, M.M., Chen, Y.: Dynamic behaviors of general N-solitons for the nonlocal generalized nonlinear Schrödinger equation. Nonlinear Dyn. **104**, 2621-2638 (2021)
[23] Ablowitz, M.J., Musslimani, Z.H.: Integrable nonlocal nonlinear Schrödinger equations, Phys. Rev. Lett. **110**, 064105 (2013)
[24] Ablowitz, M.J., Musslimani, Z.H.: Integrable nonlocal nonlinear equations, Stud. Appl. Math. **139**(1), 7-59, (2017)
[25] Pu, J.C., Li, J., Chen, Y.: Solving localized wave solutions of the derivative nonlinear Schrödinger equation using an improved PINN method. Nonlinear Dyn. **105**, 1723-1739 (2021)
[26] Akhmediev, N.N., Korneev, V.I.: Modulation instability and periodic solutions of the nonlinear Schrödinger equation. Theor. Math. Phys. **69**, 1080-1093 (1986)
[27] Zhao, L.C., Xin, G.G., Yang, Z.Y.: Rogue-wave pattern transition induced by relative frequency, Phys. Rev. E **90**, 022918 (2014)
[28] Shen, J., Geng, X. G., Xue, B.: Modulation instability and dynamics for the Hermitian symmetric space derivative nonlinear Schrödinger equation. Commun. Nonlinear Sci. Numer. Simulat. **78**, 104877 (2019)
[29] Yue, Y.F., Huang, L.L., Chen, Y.: Modulation instability, rogue waves and spectral analysis for the sixth-order nonlinear Schrödinger equation. Commun. Nonlinear Sci. Numer. Simulat. **89**, 105284 (2020)
[30] Zabusky, N.J., Kruskal, M.D.: Interaction of solitons in a collisionless plasma and the recurrence of initial states, Phys. Rev. Lett. **15**, 240-243 (1965)
[31] Nakamura, A.. Chen. H.H.: Multi-soliton solutions of a derivative nonlinear schrödinger equation. J. Phys. Soc. Jpn. **49**, 813-816 (1980)
[32] Huang, N.N., Chen. Z.Y.: Alfvén solitons. J. Phys. A: Math.Gen. **23**, 439-453 (1990)
[33] Kamchatnov. A.M.: On improving the effectiveness of periodic solutions of the NLS and DNLS equations. J. Phys. A:Math. Gen. **23**, 2945-2960 (1990)
[34] Kamchatnov, A.M., Darmanvan, S.A., Lederer. F.: Forrnation of solitons on the sharp front of the pulse in an opticaliber. Phys. Lett. A **245**, 259-264 (1998)
[35] Steudel. H.: The hierarchy of multi-soliton solutions of the derivative nonlinear Schrödinger equation. J. Phys. A: Math.Gen. **36**, 1931-1946 (2003)
[36] Guo, B.L., Ling, L.M., Liu, Q.P.: High-order solutions and generalized Darboux transformations of derivative nonlinear Schrödinger equations. Stud. Appl. Math. **130**, 317-344 (2012)

[37] Xu, T., Chen, Y.: Mixed interactions of localized waves in the three-component coupled derivative nonlinear Schrödinger equations. Nonlinear Dyn. **92**, 2133-2142 (2018)
[38] An Atlas of Oceanic Internal Solitary Waves. Global Ocean Associates,(2002)
[39] Akhmediev, N.N., Eleonskii, V.M., Kulagin, N.E.: Exact first-order solutions of the nonlinear Schrödinger equation. Theor. Math. Phys. **72**, 809-818 (1987).
[40] Hu, X.R., Lou, S.Y., Chen, Y.: Explicit solutions from eigenfunction symmetry of the Korteweg-de Vries equation, Phys. Rev. E **85**, 056607 (2012)
[41] He, J.S., Tao, Y.S., Porsezian, K., Fokas, A.: Rogue wave management in an inhomogeneous Nonlinear Fibre with higher order effects, J. Nonlinear Math. Phys. **20**, 407-419 (2013)
[42] Kedziora, D.J., Ankiewicz, A., Akhmediev, N.: Rogue waves and solitons on a cnoidal background, Eur. Phys. J-Spec. Top. **223**(1), 43-62 (2014)
[43] Huang, X., Ling, L.M.: Soliton solutions for the nonlocal nonlinear Schrödinger equation. Eur. Phys. J. Plus **131**, 148 (2016)
[44] Zhao, L.C., Ling, L.M., Qi, J.W., Yang, Z.Y., Yang, W.L.: Dynamics of rogue wave excitation pattern on stripe phase backgrounds in a two-component Bose-Einstein condensate, Commun. Nonlinear Sci. Numer. Simulat, **49**, 39-47 (2017)
[45] Chen, J.B., Pelinovsky, D.E.: Rogue periodic waves of the modified KdV equation, Nonlinearity **31**, 1955-1980 (2018)
[46] Liu, W., Zhang, Y.S., He, J.S.: Rogue wave on a periodic background for Kaup-Newell equation, Rom. Rep. Phys. **70**, 106 (2018)
[47] Xue, B., Shen, J., Geng, X.G. Breathers and breather-rogue waves on a periodic background for the derivative nonlinear Schrödinger equation. Physica Scripta, **95**(5) (2020).
[48] Zhou, H.J., Chen, Y.: Breathers and rogue waves on the double-periodic background for the reverse-space-time derivative nonlinear Schrödinger equation. Nonlinear Dyn. (2021)
[49] Zakharov, V. E., Shabat, A. B.: Interaction between solitons in a stable medium. Sov. Phys. JETP **37**, 823-828 (1973)
[50] Kuznetsov, E.A.: Solitons in a parametrically unstable plasma. Sov. Phys. Dokl. **22**, 507-508 (1977)
[51] Hasegawa, A. Kodama, Y.: Solitons in optical communications. Berlin, Germany: Springer (1995)
[52] He, J.S., Charalampidis, E.G., Kevrekidis, P.G., Frantzeskakis, D.J.: Rogue waves in nonlinear Schrödinger models with variable coefficients: Application to Bose-Einstein condensates, Phys. Lett. A **378**(56), 577-583 (2014)
[53] Wang, L., Li, M., Qi, F.H., Geng, C.: Breather interactions, higher-order rogue waves and nonlinear tunneling for a derivative nonlinear Schrödinger equation in inhomogeneous nonlinear optics and plasmas. Eur. Phys. J. D **69**, 108 (2015)
[54] Randoux, S., Suret, P., Chabchoub, A., Kibler, B., El, G.: Nonlinear spectral analysis of Peregrine solitons observed in optics and in hydrodynamic experiments, Phys. Rev. E **98**, 022219 (2018)

(HZ) School of Mathematical Sciences, Shanghai Key Laboratory of Pure Mathematics and Mathematical Practice, and Shanghai Key Laboratory of Trustworthy Computing, East China Normal University, Shanghai 200241, China

(YC) School of Mathematical Sciences, Shanghai Key Laboratory of Pure Mathematics and Mathematical Practice, and Shanghai Key Laboratory of Trustworthy Computing, East China Normal University, Shanghai 200241, China

(YC) College of Mathematics and Systems Science, Shandong University of Science and Technology, Qingdao 266590, China

Email address: ychen@sei.ecnu.edu.cn

(XT) School of Mathematical Sciences, Shanghai Key Laboratory of Pure Mathematics and Mathematical Practice, and Shanghai Key Laboratory of Trustworthy Computing, East China Normal University, Shanghai 200241, China

(YL) School of Mathematical Sciences, Shanghai Key Laboratory of Pure Mathematics and Mathematical Practice, and Shanghai Key Laboratory of Trustworthy Computing, East China Normal University, Shanghai 200241, China